



## Antarctic Circumpolar Current frontal system in the South Atlantic: Monitoring using merged Argo and animal-borne sensor data

L. Boehme,<sup>1,2</sup> M. P. Meredith,<sup>2</sup> S. E. Thorpe,<sup>2</sup> M. Biuw,<sup>1</sup> and M. Fedak<sup>1</sup>

Received 15 November 2007; revised 9 May 2008; accepted 20 June 2008; published 5 September 2008.

[1] We describe large-scale features of the Antarctic Circumpolar Current (ACC) in the Atlantic part of the Southern Ocean by merging Argo data and data obtained by novel animal-borne CTD sensors. Twenty one of these CTD-Satellite Relay Data Loggers (CTD-SRDLs) were attached to Southern elephant seals (*Mirounga leonina*) on South Georgia. The merged data yield unified gridded hydrographic fields with high temporal and spatial resolution, enabling the determination of features absent in each of the data sets separately. The structure and variability of the frontal field revealed by this data set were compared with those in daily quarter-degree, optimally interpolated sea surface temperature fields and fields of weekly gridded sea level anomaly. In general, the frontal positions derived using our data set are in agreement with previous work, especially where the pathways are constrained by topography, e.g., at the North Scotia Ridge and the South Scotia Ridge. However, with the improved temporal and spacial resolution provided by the CTD-SRDLs, we were able to observe some novel features. All frontal positions are more variable than previously indicated across the Scotia Sea and west of the Mid-Atlantic Ridge on seasonal time scales. The merged data set shows the temporal variability of the Southern ACC Front (SACCF) north of South Georgia and in its position east of the island, where the SACCF lies further north than has been suggested in previous work. In addition, the Subantarctic Front crosses the Mid-Atlantic Ridge about 400 km further north when compared to previous work.

**Citation:** Boehme, L., M. P. Meredith, S. E. Thorpe, M. Biuw, and M. Fedak (2008), Antarctic Circumpolar Current frontal system in the South Atlantic: Monitoring using merged Argo and animal-borne sensor data, *J. Geophys. Res.*, *113*, C09012, doi:10.1029/2007JC004647.

### 1. Introduction

[2] The most pronounced feature of the Southern Ocean circulation is the eastward flow of the Antarctic Circumpolar Current (ACC), which plays a crucial role in the global climate system by connecting the major oceans and redistributing oceanic properties, such as heat, salt and nutrients [Rintoul *et al.*, 2001]. This flow is also associated with a steep rise of isopycnals toward the south through the entire water column. This poleward rise of isotherms and isohalines is not uniform, but occurs in a series of clear step-like patterns. Between zones of relatively uniform water mass properties lie bands of large horizontal density gradients characterizing the ACC fronts, which are associated with relatively narrow, deep-reaching current cores and large surface velocities [Nowlin *et al.*, 1977; Nowlin and Clifford, 1982; Nowlin and Klinck, 1986]. Understanding the structure and location of the major fronts of the Southern Ocean

is of considerable importance because of their influence on climate and ecosystem processes.

[3] Using historical data, Orsi *et al.* [1995] and Belkin and Gordon [1996] were the first to map the circumpolar distribution of the Southern Ocean fronts. From north to south, the fronts and zones of the Southern Ocean are: the Subtropical Front (STF), Subantarctic Zone (SAZ), Subantarctic Front (SAF), Polar Frontal Zone (PFZ), Polar Front (PF), Antarctic Zone (AAZ), Southern ACC Front (SACCF), Southern Zone and the southern boundary of the ACC (SB) [Whitworth, 1980; Orsi *et al.*, 1995]. A variety of definitions based on water mass properties have been used to identify these fronts (see works of Orsi *et al.* [1995] and Belkin and Gordon [1996] for useful summaries of these definitions). However, the frontal properties are not uniform in all sectors of the Southern Ocean. The variations in frontal structure from region to region and the multiplicity of definitions used by various authors have led to some confusion in identifying particular fronts. In addition, many areas have remained relatively poorly sampled and in very few locations have sufficient repeat measurements been made to permit the variability of the fronts to be assessed. These earlier studies were based on ship-based measurements with their high accuracy and depth-resolving capability, but these data are scarce in the Southern Ocean and

<sup>1</sup>NERC Sea Mammal Research Unit, University of St. Andrews, St. Andrews, UK.

<sup>2</sup>British Antarctic Survey, Natural Environment Research Council, Cambridge, UK.

are focused on the summer season on the basis of inherent logistic difficulties.

[4] Others studies [e.g., *Gille, 1994; Moore et al., 1999; Kostianoy et al., 2003*] have also examined the time-varying frontal locations on a circumpolar scale using satellite measurements. Indeed, the spatial and temporal resolution of the altimetric sea surface height (SSH) measurements used by e.g. *Gille [1994]* were coarse compared to other satellite data. *Moore et al. [1999]* determined the surface PF location from weekly composites of the daily images of sea surface temperature (SST) measured from satellite-borne infrared sensors hampered by cloud cover. *Dong et al. [2006]* use the recently launched Advanced Microwave Scanning Radiometer for the Earth Observing System (AMSR-E), which provides global all-weather SST measurements, though with lower spatial resolution than more traditional infrared SST. More recently, *Sokolov and Rintoul [2007]* used weekly maps of SSH to characterize the structure and variability of the ACC fronts and filaments south of Australia.

[5] The studies based on remote SST were limited to analyses of fronts with a surface expression in SST and only a few studies were able to collect in-situ data with a sufficient temporal resolution to investigate the frontal variability using the subsurface expressions [*Sokolov and Rintoul, 2002; Thorpe et al., 2002; Meredith et al., 2003b; Sokolov et al., 2006*]. None of these studies describe the three major fronts of the ACC (SAF, PF and SACCF) simultaneously with good spatial and temporal coverage. *Sokolov and Rintoul [2007]* are the first to describe the multiple jets of the ACC associated with these three fronts together using weekly SSH maps. Here, we use a comprehensive in-situ data set collected during 2004 and 2005 to determine the location, structure and variability of the three major fronts in the South Atlantic sector of the Southern Ocean (Figure 1). We focus on data obtained by free-drifting profiling floats seeded by the Argo project [*Gould et al., 2004*] and complement these data with hydrographic profiles recorded by animal-borne sensors.

[6] Argo is a global array of autonomous profiling floats that provides vertical profiles of salinity and temperature of the upper 2000 dbar of the open ocean at 10-day intervals. This array samples the seasons evenly, so the measurements are not biased toward seasons favorable for ship-based work [*Gould et al., 2004*]. Although the profiling float has enormous potential for broad-scale ocean observations, it does not provide a complete observational strategy. The coverage of floats in the Southern Ocean is sparser than elsewhere especially the seasonally ice-covered regions.

[7] Marine mammals, however, can help to overcome these limitations and provide a complementary high-resolution data source [*Boehme et al., 2008*]. They can operate deep in ice-covered regions [*Lydersen et al., 2004*] and animal-borne sensors can accurately record hydrographic data at high frequency and in near real-time from remote, relatively inaccessible parts of the ocean [*Lydersen et al., 2004; Charrassin et al., 2004; Bailleul et al., 2007; Biuw et al., 2007*]. Autonomous CTD-Satellite Relay Data Loggers (CTD-SRDLs) can be attached to marine animals and report vertical profiles of salinity, temperature and pressure to a depth of up to 2000 m. Enlisting marine animals as sampling platforms is not a new idea. The earliest published

reference to this approach is from 1970 [*Evans, 1970*]. However, until recently, no one had ever developed the technology to allow collection of high-quality CTD information. Nowadays, these instruments have the potential to collect information about the oceans that is not only relevant to the study of the ecology of animals carrying the instruments [e.g., *Biuw et al., 2007*], but also for studying the physical structure of the oceans [*Lydersen et al., 2002, 2004; Charrassin et al., 2004; Boehme et al., 2008*]. While CTD-SRDL measurements are neither regular in terms of spatial and temporal coverage (compared, for example, with satellite measurements of oceanographic fields) nor completely random (such as those from drifting buoys), these studies provide valuable in-situ information about the subsurface structure of the ocean. Accurate satellite positioning of diving marine animals, high-accuracy sensors, and the potential to collect large numbers of profiles cost-effectively make these studies particularly important in regions where traditional oceanographic measurements are scarce. CTD-SRDLs can be programmed to sample and transmit hydrographic profiles on a daily basis and are therefore intrinsically an eddy-resolving device, rather than a broad-scale one. The natural niche for CTD-SRDLs in the observing system is in providing complementary measurements of boundary currents and fronts, as well as coverage of undersampled ocean basins. They thus provide a powerful complement to existing methods rather than a replacement for them [*Boehme et al., 2008*]. Only by combining these two data sets, we are able to investigate the variability of the frontal system from Drake Passage to the Mid-Atlantic Ridge on short temporal scales.

[8] In this paper, we describe the characteristics of the combined data set and methods we used to identify the SAF, PF and SACCF, including the optimal interpolation method used to calculate gridded fields of temperature on selected pressure levels. Then, we use the gridded horizontal fields to determine the mean position and variability of the fronts. Finally we discuss the findings in the broader Southern Ocean context.

## 2. Data and Methods

### 2.1. Hydrographic In-Situ Data

[9] Between 2004 and 2005, more than 120 profiling floats populated the southern South Atlantic Ocean as part of the Argo project. One disadvantage of sampling by autonomous floats is that most of the measurements are without accompanying ship-board data for absolute calibration. This deficiency is especially problematic for salinity, as conductivity cells are prone to changes that can cause sensor drifts in float salinity measurements. Several methods for post-deployment quality control are available to adjust possible sensor drifts by comparison with ship-board CTD data or statistical estimates of background temperature and salinity relations [*Wong et al., 2003; Boehme and Send, 2005*]. In this study, we only used profiles that passed the Argo real-time quality control, containing information on their position, date, temperature (T) and salinity (S) profiles, with their first measurement point shallower than 20 m (Figure 2). We used either the delayed-mode data or, if not available, we used the method of *Boehme and Send [2005]* to check the float salinity for any drifts.

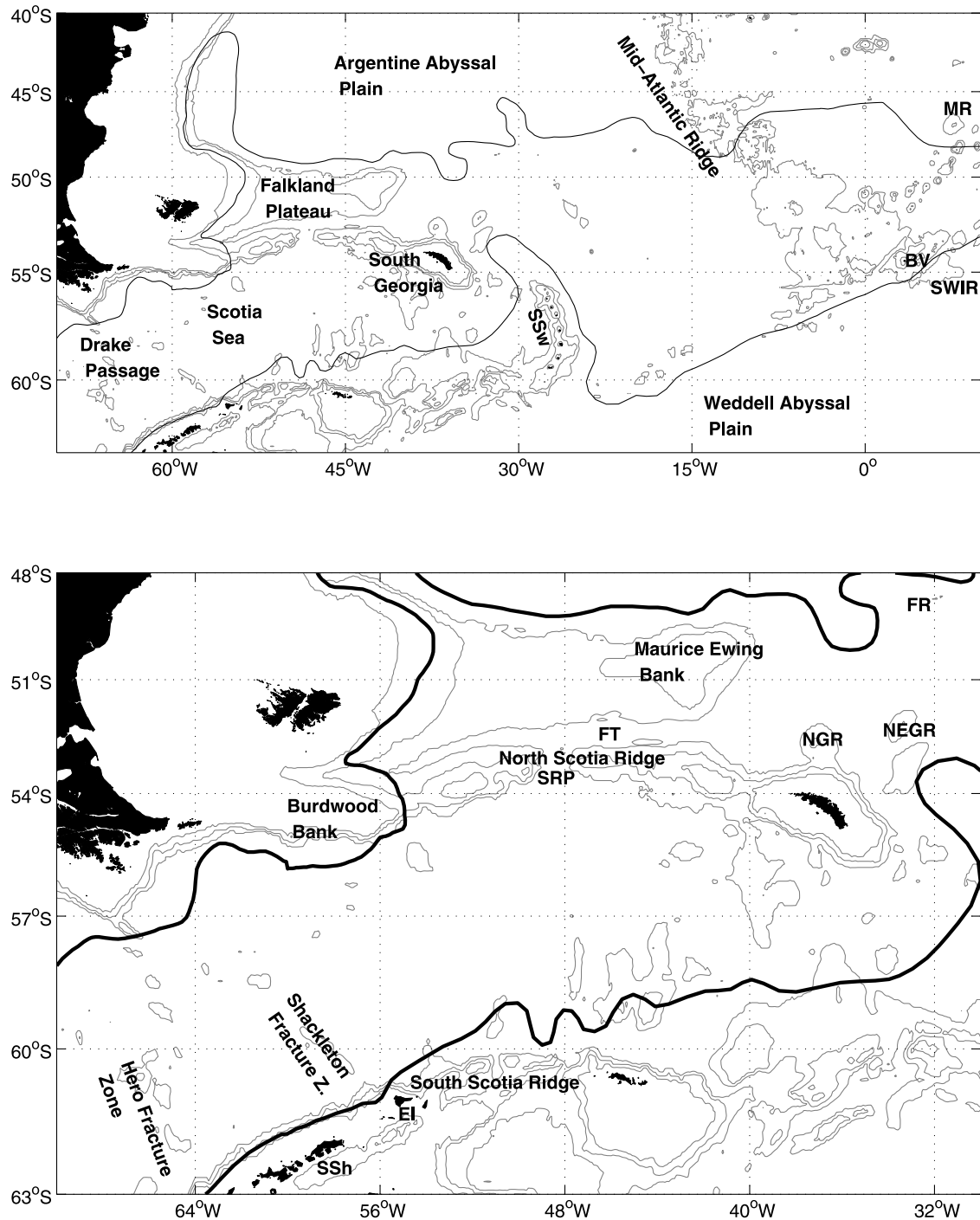


**Figure 1.** Schematic of the southern South Atlantic (top) and the Scotia Sea (bottom). Some important topographic features are marked: Meteor Rise (MR), Bouvetøya (BV), South West Indian Ridge (SWIR), South Sandwich Islands (SSw), Falkland Ridge (FR), Falkland Trough (FT), Northwest Georgia Rise (NGR), Northeast Georgia Rise (NEGR), Shag Rocks Passage (SRP), Elephant Island (EI) and South Shetland Islands (SSh). The 1000, 2000, and 3000 m isobaths are marked. The two solid lines show the extent of the ACC. The northern line corresponds to the SAF and the southern line to the SB from *Orsi et al.* [1995].

[10] Our CTD-SRDL data come from the SEaOS project (Southern Elephant Seals as Oceanographic Samplers), an international interdisciplinary program aimed at increasing our understanding of how Southern elephant seals interact

with their physical environment and also at demonstrating and implementing this cost-effective means of gathering routine observations of hydrographic data from remote environments [*Biuw et al.*, 2007; *Boehme et al.*, 2008].

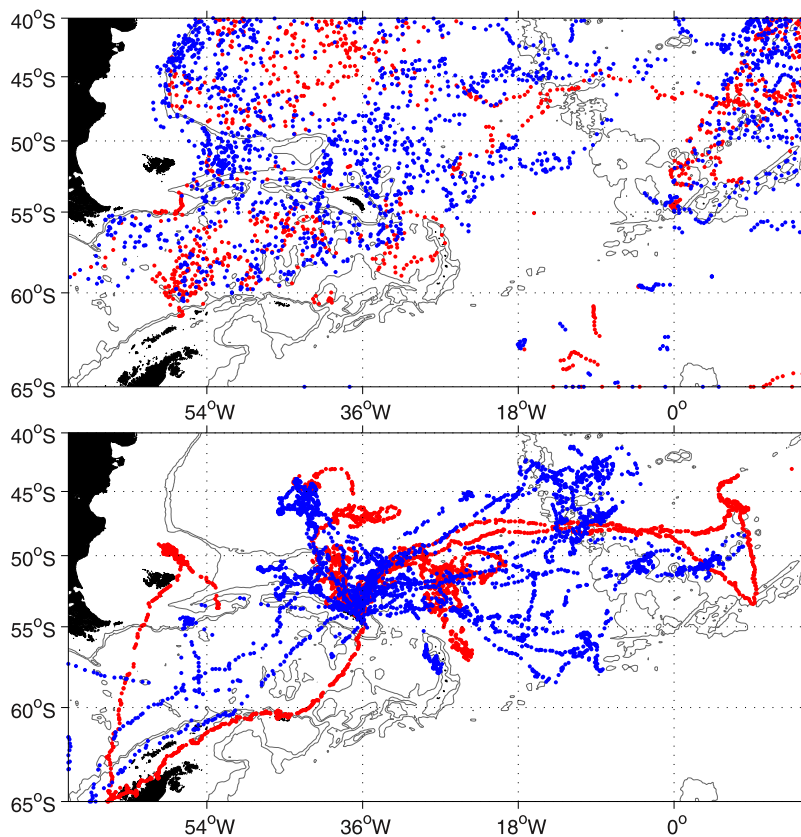


**Figure 2.** Spatial distribution of Argo float data (top) and CTD-SRDL data (bottom) in the years 2004 (red) and 2005 (blue).

During the SEaOS program, we used CTD-SRDLs, custom-built by the Sea Mammal Research Unit, St Andrews, UK and Valeport Ltd., Devon, UK. We deployed 6 CTD-SRDLs and 2 temperature only SRDLs in 2004 and 13 CTD-SRDLs in 2005 at Husvik, South Georgia ( $54^{\circ} 11' S$ ,  $36^{\circ} 42.5' W$ ). The CTD-SRDLs were fixed harmlessly to seals' fur after the elephant seals completed their annual moult in January/February. The CTD-SRDLs were set to ensure batteries lasted throughout as much of the winter migration as possible, ideally until seals returned to breed in September. During the animals' migration the CTD-SRDLs recorded and transmitted hydrographic profiles at a rate of approximately 2 profiles/day to an average depth of about 560 m, representing a combination of transect-type sections with a spatial resolution of 25–50 km along the migratory routes and mooring like data in the foraging areas of the seals [Biuw *et al.*, 2007; Boehme *et al.*, 2008]. The CTD-SRDLs were finally lost, when the animals moulted again. In 2004 and 2005, we obtained more than 8200 hydrographic profiles to depths up to 2000 m, from the Drake Passage to east of the Mid-Atlantic Ridge (Figure 2).

[11] CTD-SRDLs are checked in a calibration facility before deployment and these comparisons yield errors of less than 2 mK in temperature and less than 0.003 mS/cm in conductivity leading to salinity values with an error up to about 0.010 in the worst case scenario. Figure 3 shows differences between a ship-based CTD (SBE 911) and a CTD-SRDL, which was attached to the frame of the ship-based instrument. Only data measured in a homogeneous

layer were used to compare both instruments. The differences in temperature are less than 5 mK and the resolution of the temperature data is obvious. The salinity data recorded by the CTD-SRDL is also within 0.005 of the measurements taken by the SBE 911 (Figure 3). Such direct comparisons between ship-based CTDs and CTD-SRDLs were performed for some of the deployed instruments. In order to properly quantify possible sensor drifts during the deployment with high accuracy, recovery of the CTD-SRDL and recalibration of its sensors would be necessary. However, since a recalibration is generally not possible on a routine basis, CTD-SRDL data have to be checked in an indirect way. Again, a method similar to Boehme and Send [2005] has been created and implemented to compare the CTD-SRDL measurements with historical CTD data and calibrated Argo float data to correct any sensor drifts and possible offsets in temperature and salinity (L. Boehme *et al.*, unpublished data, 2008). All deployed CTD-SRDLs have no sensor drift or offset in temperature during their lifetime, but the salinity measurements have often an offset in the order of 0.1, which is traced back to the influence of the seals head on the external field of the inductive cell. All data were checked and corrected for such offset. This post-deployment quality control adds an uncertainty to the data set, which is typically in the order of 0.005 in salinity [Wong *et al.*, 2003; Boehme and Send, 2005], but can be higher in data sparse regions (L. Boehme *et al.*, unpublished data, 2008). Hence we have to add an uncertainty to the data, but expect the CTD-SRDL data to be better than 0.02 in

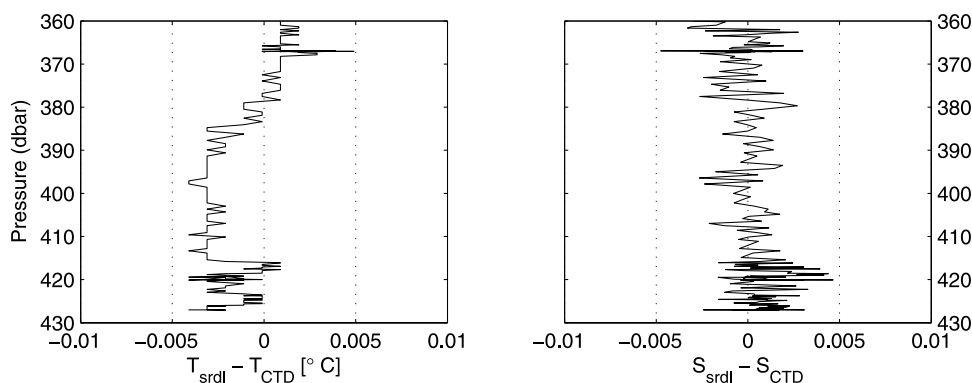


**Figure 3.** Differences in temperature (left) and salinity (right) of a CTD-SDRL and a ship-based CTD. The CTD-SRDL was attached to the frame of the ship-based instrument. Only measurements taken in a homogeneous water mass are used.

temperature and salinity, which is of at least the same quality as XBT data [Boyd and Linzell, 1993].

[12] Figure 2 shows the complementarity of the two data sets (Argo and CTD-SRDLs), especially in the area between South Georgia and the Mid-Atlantic Ridge. These two data sources produce a data set with a temporal and spatial resolution, which were previously unavailable. This data set includes up to 1000 hydrographic profiles per month (Figure 4), of which CTD-SRDLs contribute up to 90%. Figure 4 shows a reduction in the number of monthly profiles, when the CTD-SRDLs stopped working between September and December each year. The spatial resolution of each subset also changed from less than 20 km to more than 60 km, when less profiles were present. With reference to Figure 4, it can be seen that the Argo float data provide the background field, and the CTD-SRDL data are used to increase the temporal and spatial resolution of the data set, yet the only source of data between the South Sandwich Islands and the Mid-Atlantic Ridge (Figure 2).

[13] This combined data set was then used to generate gridded horizontal potential temperature ( $\Theta$ ) fields on pressure levels using an optimal interpolation scheme similar to the one introduced by Boehme and Send [2005] (see Appendix). For all calculations we used a  $0.4^\circ \times 0.25^\circ$  grid ( $\sim 25$  km) from  $80^\circ\text{W}$  to  $15^\circ\text{E}$  and  $63^\circ\text{S}$  to  $40^\circ\text{S}$  at 200 dbar, 300 dbar and 500 dbar pressure. We also calculated  $\Theta$  of the temperature minimum layer closest to the surface. All data without any temporal separation were used to investigate the mean field of the two year period from 2004 to 2005. For the monthly temperature fields we used the detected temporal scale  $\tau$  (see Appendix). For each

monthly field, all available data of the two year period were used, but each measurement was also weighted by  $\tau$  (see Appendix) centered around the middle of the specific month. Hence the data coverage is the same for the mean field and each monthly field, but when sufficient data in time were available, the monthly fields reflects these data and such regions deviate from the mean field [Boehme and Send, 2005]. This fall back on the mean field, when no data close in time is available, is rather underestimating any variations from the meanfield and will result in little variation between monthly maps in regions with few profiles.

## 2.2. Sea Surface Temperature

[14] We also used an optimally interpolated daily, quarter degree ( $\pm 25$  km) SST product (<http://www.ssmi.com>). This product is computed by a combination of two satellites, the TRMM Microwave Imager (TMI) and NASDA's Advanced Microwave Scanning Radiometer for EOS (AMSR-E). TMI and AMSR-E observations are used to retrieve SST and this combination provides nearly complete global coverage each day. The accuracy of this SST is of the order of  $\pm 0.5^\circ\text{C}$  [Gentemann et al., 2004]. Two years (January 2004 to December 2005) of daily SST observations are used in this study. Following Moore et al. [1999] and Dong et al. [2006], we used the daily SST data to calculate the standard deviation of SST and derived the mean SST gradient  $\delta\text{SST} = \sqrt{(\delta T/\delta x)^2 + (\delta T/\delta y)^2}$  including its standard deviation at the frontal positions derived from the hydrographic data.

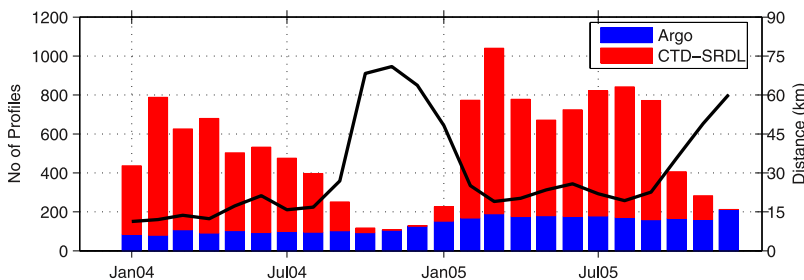


**Figure 4.** Monthly number of hydrographic profiles (bars) and mean distance to the neighboring profile (line) from the combined Argo/SRDL data set.

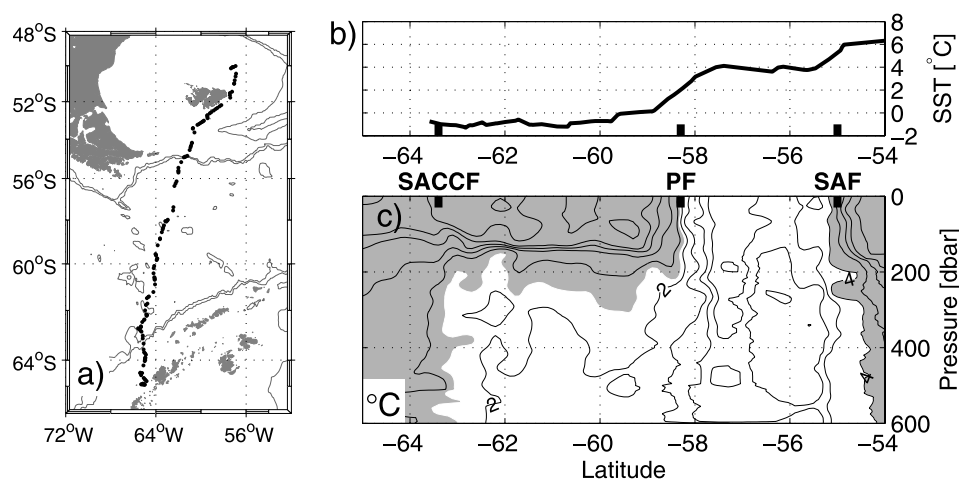


**Figure 5.** (a) Station locations from a CTD-SRDL between 7 June 2004 and 24 June 2004. Isobaths are 2000 and 3000 m and land is shaded. (b) High-resolution satellite SST interpolated onto profile location and time. (c) In-situ temperature along the animal's migration. Contour intervals every  $0.5^{\circ}\text{C}$  and areas below  $1.8^{\circ}\text{C}$  and above  $4^{\circ}\text{C}$  are shaded. Front locations are marked on the upper axis. SACCF, Southern ACC Front; PF, Polar Front; SAF, Subantarctic Front.

### 2.3. Sea Level Anomaly

[15] Satellite altimeter sea level anomaly (SLA) data were obtained from AVISO on a  $1/3^{\circ}$  Mercator grid at 7 day intervals [Ducet *et al.*, 2000]. These are multimission gridded sea surface heights computed with respect to a seven-year mean and consist of processed data from different altimeter missions (Jason-1, T/P, ENVISAT, GFO, ERS1/2 and GEOSAT). Combining data from different missions significantly improves the estimation of mesoscale signals [Le Traon and Dibarboure, 1999; Le Traon *et al.*, 2001]. We used data from August 2001 to June 2006 in this study to calculate the SLA variance.

## 3. Results

### 3.1. Definition and Determination of Fronts

[16] Fronts are identified by apparent horizontal gradients at various depth levels [Orsi *et al.*, 1995; Belkin and Gordon, 1996]. However, the particular frontal properties can change both in time and space due to air-sea interaction and cross-frontal mixing [Belkin and Gordon, 1996]. To minimize these effects, one needs a database of sufficient spatial resolution. Belkin and Gordon [1996] suggest that a distance of less than 200 km between measurements should be used, which we easily achieve with our combined data set (Figure 4). In the present paper, we use the data set of temperature and salinity profiles provided by CTD-SRDLs combined with the Argo data to describe the properties and positions of three major fronts of the ACC. First, we show CTD-SRDL data to determine the frontal properties.

[17] Figure 5 presents a section across the Drake Passage measured between 7 June 2004 and 24 June 2004 by a temperature only SRDL. This is the location most routinely sampled by ships in the Southern Ocean, and hence the one at which the frontal structures are best known. Note, however, that most historical sections have been performed during the months of the austral summer, when ship-based operations are easiest. As typically seen in meridional sections across the ACC, the temperature decreases to the

south in a series of steps or fronts, separated by zones of weaker meridional gradient. This winter section shows clear horizontal temperature gradients, which are associated with the SAF at about  $55^{\circ}\text{S}$  very close to the Burdwood Bank, the PF at about  $58^{\circ}\text{S}$  and the SACCF close to the continental shelf at about  $63.6^{\circ}\text{S}$ . In this figure, the SAF is associated with the vertical  $4^{\circ}\text{C}$  isotherm, while the PF is associated with the vertical  $2^{\circ}\text{C}$  isotherm above 200 dbar. The mixed layer south of the PF does not show any evidence of the SACCF, while below the thermocline the SACCF is shown by the vertical  $1.8^{\circ}\text{C}$  isotherm below 200 dbar (Figure 5c). These relationships between subsurface temperature and fronts agree with definitions made in previous work [e.g., Orsi *et al.*, 1995]. The satellite SST data in Figure 5b also show no evidence of the SACCF, while the other two fronts are clearly seen in the meridional temperature gradients from  $0^{\circ}\text{C}$  to  $4^{\circ}\text{C}$  (PF) and  $4^{\circ}\text{C}$  to  $6^{\circ}\text{C}$  (SAF).

[18] Between 14 January 2005 and 26 February 2005, a CTD-SRDL recorded a hydrographic section further to the east and north from South Georgia ( $54^{\circ}\text{S}$ ,  $36^{\circ}\text{W}$ ) to the Mid-Atlantic Ridge at  $43^{\circ}\text{S}$ ,  $17^{\circ}\text{W}$  (Figure 6a). This section did not cross the ACC perpendicularly, but Figure 6e shows the strong horizontal density gradients associated with the SAF and PF at  $47^{\circ}\text{S}$  and  $49.5^{\circ}\text{S}$ , respectively. There was a loop of the SACCF at the southern end of the section (Figure 6). This northward loop of the SACCF is marked by the  $\Theta$  minimum at around 150 m and the doming of the isopycnals between  $54^{\circ}\text{S}$  and  $52^{\circ}\text{S}$  in Figure 6e. The PF is again associated with the vertical  $2^{\circ}\text{C}$  isotherm in the  $\Theta_{\min}$  layer (Figure 6c). The surface expression of the PF is very weak with only a low satellite SST gradient of about  $1^{\circ}\text{C}$  (Figure 6b). The SAF however has a clear increase of satellite SST from  $7^{\circ}\text{C}$  to  $10^{\circ}\text{C}$ . In Figure 6c, the subsurface expression of the SAF correlates with the descent of the  $4^{\circ}\text{C}$  isotherm from 100 dbar to 350 dbar to the north.

[19] At the beginning of winter 2004, a CTD-SRDL sampled a meridional section northeast of Bouvetoya from  $54^{\circ}\text{S}$ ,  $9^{\circ}\text{E}$  to  $45^{\circ}\text{S}$ ,  $5^{\circ}\text{E}$  (Figure 7a). While there was no

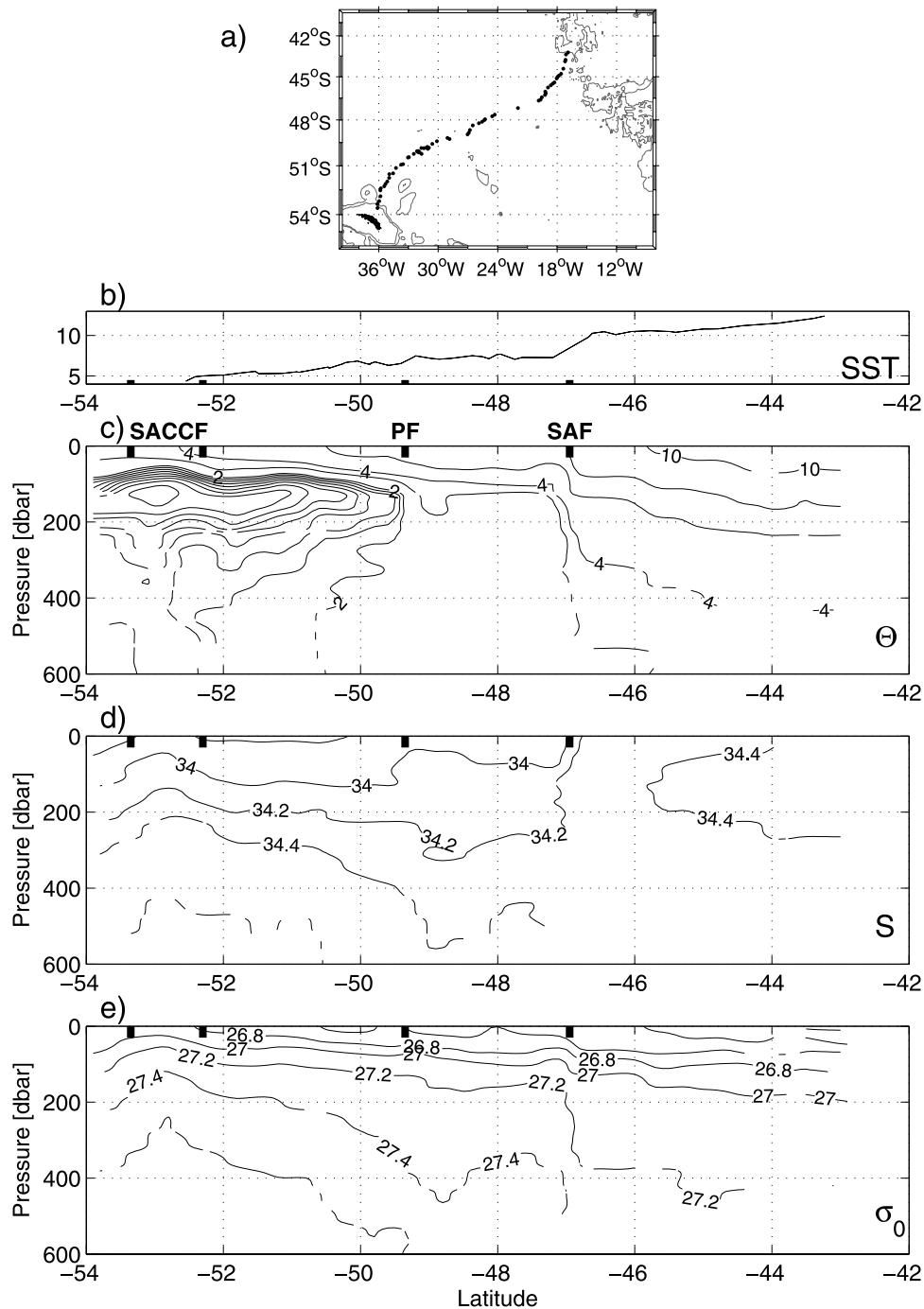


**Figure 6.** (a) Station locations from a CTD-SRDJ between 14 January 2005 and 26 February 2005. Isobaths are 2000 and 3000 m and land is shaded black. (b) High-resolution satellite SST interpolated onto profile location and time. (c) Potential temperature along the animal's migration. Contour intervals are every 0.2°C to 2°C then 3°C, 4°C and then every 2°C. Front locations are marked on the upper axis. **PF**, Polar Front; **SAF**, Subantarctic Front. (d) Salinity along the animal's migration. Contour intervals are every 0.2. (e) Potential density relative to surface pressure. Contour intervals are every 0.2 kg/m<sup>3</sup>.

obvious satellite SST gradient marking the frontal positions (Figure 7b), the subsurface hydrography in Figure 7 reveals two of the three major ACC fronts. In this figure, the SACCF is marked by vertical 1.6°C to 2°C isotherms from the surface to below 600 dbar and a horizontal density gradient (Figure 7e). The temperature minimum layer at

around 200 dbar is broken up to the north at around 49.5°S (Figure 7c). A small cold water patch ( $\Theta < 2^\circ\text{C}$ ) is found at 49°S. The northern end of this patch is also marked by a near vertical potential density isopycnal of  $\sigma_0 = 27.4 \text{ kg/m}^3$ , indicating the PF at 48.7°S (Figure 7e).

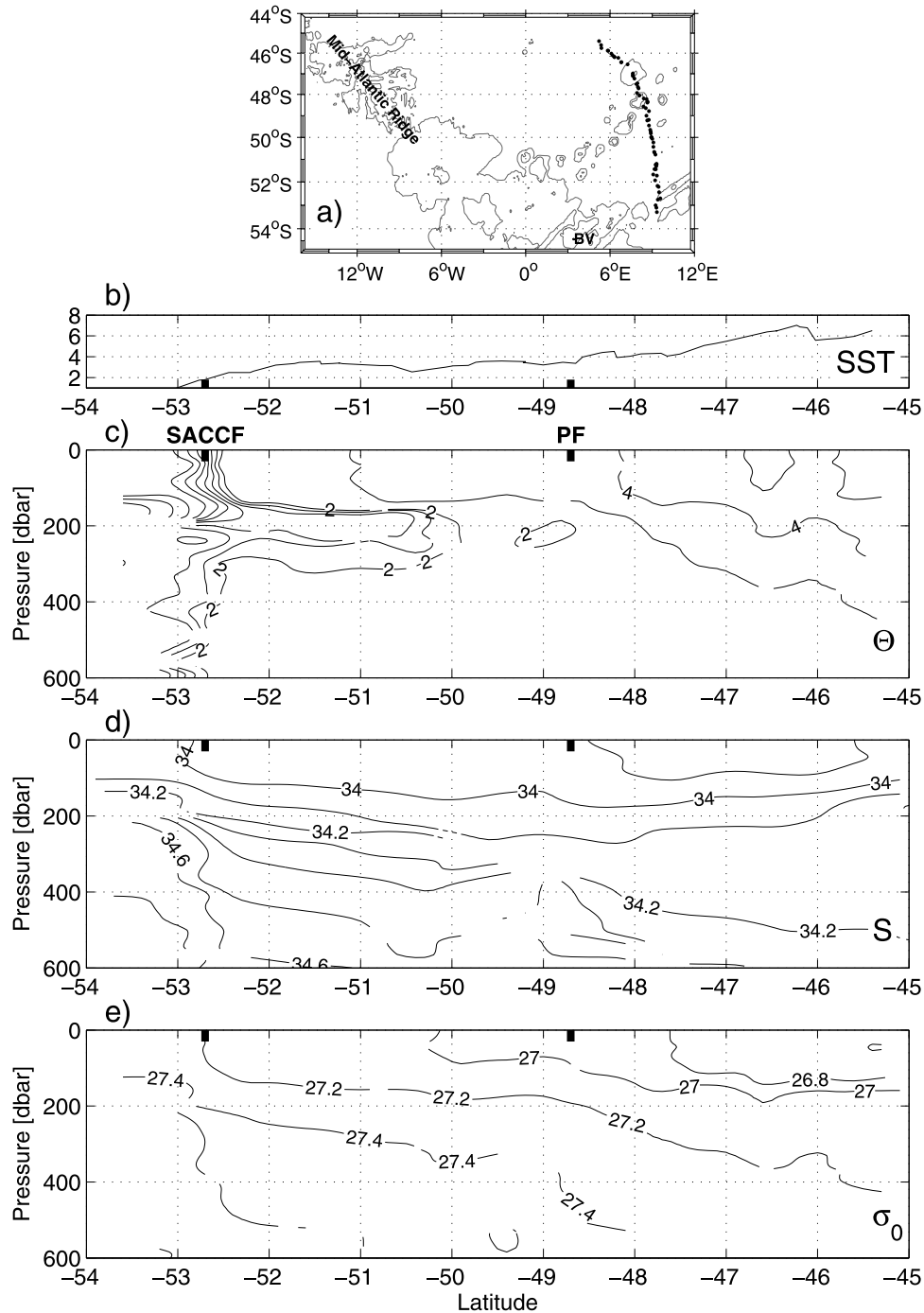


**Figure 7.** (a) Station locations from a CTD-SRDL between 13 April 2004 and 4 May 2004. Isobaths are 2000 and 3000 m. Bouvetøya is highlighted (BV). (b) High-resolution satellite SST interpolated onto profile location and time. (c) Potential temperature along the animal's migration. Contour intervals are every 0.2°C to 2°C, then 3°, 4° and every 2°C. Front locations are marked on the upper axis. **SACCF**, Southern ACC Front; **PF**, Polar Front. (d) Salinity along the animal's migration. Contour intervals are every 0.1. (e) Potential density relative to surface pressure. Contour intervals are every 0.2 kg/m<sup>3</sup>.

[20] The  $\Theta$ -S properties within fronts can change along-stream [Belkin and Gordon, 1996]. This can be seen in the different salinities between the section from South Georgia to the Mid-Atlantic Ridge (Figure 6d) and the section further to the east (Figure 7d) with its higher salinities in the PFZ. However, the temperature ranges belonging to

certain fronts were very stable in our area of interest, so we choose to define the frontal positions on the basis of temperature criteria at given depth levels (Table 1). We found the SAF's axial indices to be very stable in our area of interest with a vertical 4°C isotherm from 150 dbar to 350 dbar. This is slightly different from previous work

**Table 1.** Summary of Front Indicators of the ACC in the South Atlantic Used in This Paper

Front	Sub-surface Criteria	Satellite SST Criteria
SAF	$\Theta = 4.0^{\circ}\text{C}$ at $p = 300$ dbar	SST gradient
PF	$\Theta = 2.0^{\circ}\text{C}$ in $\Theta_{\min}$ layer (100–300 m) or $\Theta = 2.0^{\circ}\text{C}$ at $p = 200$ dbar	SST gradient can be weak
SACCF	$\Theta = 1.8^{\circ}\text{C}$ at $p = 500$ dbar	most times no SST gradient

<sup>a</sup>The last column indicates whether an SST gradient can be utilized to locate a front.

[Peterson and Whitworth, 1989; Orsi et al., 1993, 1995], but proved to be the best indicator in our area and time period. The criterion for identification of the PF is similar to that used in previous work [Botnikov, 1963; Belkin and Gordon, 1996]. The vertical  $2^{\circ}\text{C}$  isotherm in the  $\Theta_{\min}$  layer is an indicator of the PF almost everywhere in the Southern Ocean and is in agreement with the definition of the PF as the location of rapid descent of the  $\Theta_{\min}$  by Gordon [1971]. Detailed descriptions of the hydrographic subsurface properties are scarcer for the SACCF than for the SAF or PF. The SACCF, as with the other ACC fronts, is identified by large horizontal density gradients through the water column (Figures 6 and 7). The northern limit of the front can be identified from horizontal changes in the properties of Upper Circumpolar Deep Water (UCDW), a type of the Circumpolar Deep Water that occupies most of the deep layers of the ACC [Sievers and Nowlin, 1984]. From analysis of historical hydrographic sections, Orsi et al. [1995] locate stations north of the SACCF by a potential temperature greater than  $1.8^{\circ}\text{C}$  along the temperature maximum of the UCDW at depths greater than 500 m. It is apparent that this large-scale criterion presented does not provide a reliable indicator for the position of the SACCF in local areas (as shown previously by Thorpe et al. [2002] and Meredith et al. [2003b]) and it has been shown at other locations that the fronts change along-stream as they split and merge and are subject to seasonal cycles in heat and freshwater flux [e.g., Belkin and Gordon, 1996]. Notwithstanding this, the  $\Theta = 1.8^{\circ}\text{C}$  isotherm at 500 dbar pressure proved to be the best indicator to track the SACCF in our area of interest and time period.

[21] To map the frontal positions, we used the gridded potential temperature fields and extracted the dedicated isotherm for each front as described in Appendix. For the position of the SAF, we used the position of the  $\Theta = 4.0^{\circ}\text{C}$  isotherm at a pressure ( $p$ ) of 300 dbar. For the PF we extracted the  $\Theta = 2.0^{\circ}\text{C}$  isotherm in the  $\Theta_{\min}$  layer and, if not present, the  $\Theta = 2.0^{\circ}\text{C}$  isotherm at  $p = 200$  dbar pressure. The SACCF was located by selecting the  $\Theta = 1.8^{\circ}\text{C}$  isotherm at  $p = 500$  dbar pressure (Table 1).

### 3.2. Frontal Positions

#### 3.2.1. Subantarctic Front

[22] The mean position of the SAF for the years 2004 and 2005 derived from our merged data set corresponds very well with the position of Orsi et al. [1995] in the western part of the study region, while the position in the eastern part lies further north. The path of the SAF is constrained by the bathymetry (Figure 8). In Figure 8, the SAF flows close

to the northern shelf slope in the western part of Drake Passage until it reaches  $60^{\circ}\text{W}$ . Here, south of Burdwood Bank, the SAF moves away from the shelf slope before turning northward. The SAF crosses the North Scotia Ridge and the Falkland Trough before the SAF follows the 1500 m depth contour on the west side of the Argentine Abyssal Plain as the Malvinas Current. At  $40^{\circ}\text{S}$  the SAF retroflects upon encountering the Brazil Current. The SAF then flows southward at about  $55^{\circ}\text{W}$  until it is shifted eastward and flows north of the Falkland Plateau and the Falkland Ridge along  $48^{\circ}\text{S}$ . During this southward movement the SAF starts to meander. Further to the east the mean SAF position of Orsi et al. [1995] shows two big loops to the south and north, which are not represented by our mean position of the SAF. The SAF crosses the Mid-Atlantic Ridge at  $45^{\circ}\text{S}$ ,  $15^{\circ}\text{W}$ .

[23] The monthly SAF positions (Figures 8b and 8c) reveal areas with high variability and their differences between 2004 and 2005. The path from south of the Burdwood Bank crossing the Falkland Plateau and the position along the Brazil/Malvinas Confluence seems always to be an area of higher variability of the frontal position. The areas of higher variability east of the Maurice Ewing Bank shifted from the western part ( $45^{\circ}\text{W}$ – $30^{\circ}\text{W}$ ) in 2004 to the eastern part ( $30^{\circ}\text{W}$ – $15^{\circ}\text{W}$ ) in 2005. The path of the SAF across the Mid-Atlantic Ridge seems to be strongly constrained by the underlying topography as indicated by a very small variability in the frontal positions (Figures 8b and 8c).

#### 3.2.2. Polar Front

[24] Our derived position of the PF lies mostly north of the position of the PF of Moore et al. [1999] and corresponds well with the PF of Orsi et al. [1995] (Figure 9a). As with the SAF, the path of the PF is also controlled by the topography. In Figure 9a, the mean path of the PF starts west of Drake Passage south of  $60^{\circ}\text{S}$ , but north of the Hero Fracture Zone at  $66^{\circ}\text{W}$ . It then continues to the northeast until it reaches the North Scotia Ridge. Then it loops eastward into a meander to the east end of the ridge until it finds a way through the Shag Rocks Passage to the north toward the Maurice Ewing Bank. Here, the position of the PF lies further to the east than indicated in Orsi et al. The PF then flows across the bank looping to the east and following the  $50^{\circ}\text{S}$  parallel. At  $50^{\circ}\text{S}$ ,  $10^{\circ}\text{W}$  the PF is shifted to the north crossing the Mid-Atlantic Ridge. It then loops back to the southeast and follows again the  $50^{\circ}\text{S}$  parallel (Figure 9a).

[25] All the monthly positions of the PF follow this mean path (Figures 9b and 9c), but show a much greater variability than the monthly SAF positions (Figures 8b and 8c). In 2004, the PF showed a big northward loop at  $65^{\circ}\text{W}$  before continuing to the northeast with less variability. During 2004, the PF increased the eastward loop to the south of the North Scotia Ridge before crossing the North Scotia Ridge through the Shag Rocks Passage (Figure 9b). After looping cyclonically around the Maurice Ewing Bank, it then meandered to the east with strong variability of up to  $3^{\circ}$  in latitude between  $35^{\circ}\text{W}$  and  $18^{\circ}\text{W}$ . Constrained by the topography, it crossed the Mid-Atlantic Ridge at  $50^{\circ}\text{S}$ ,  $10^{\circ}\text{W}$ , before looping northward above the Mid-Atlantic Ridge.

[26] In 2005, the PF did not show the northward movement at  $65^{\circ}\text{W}$ , but stronger variability within Drake Passage (Figure 9c). The loop to the west before crossing the North Scotia Ridge diminished in 2005. On its way north to the

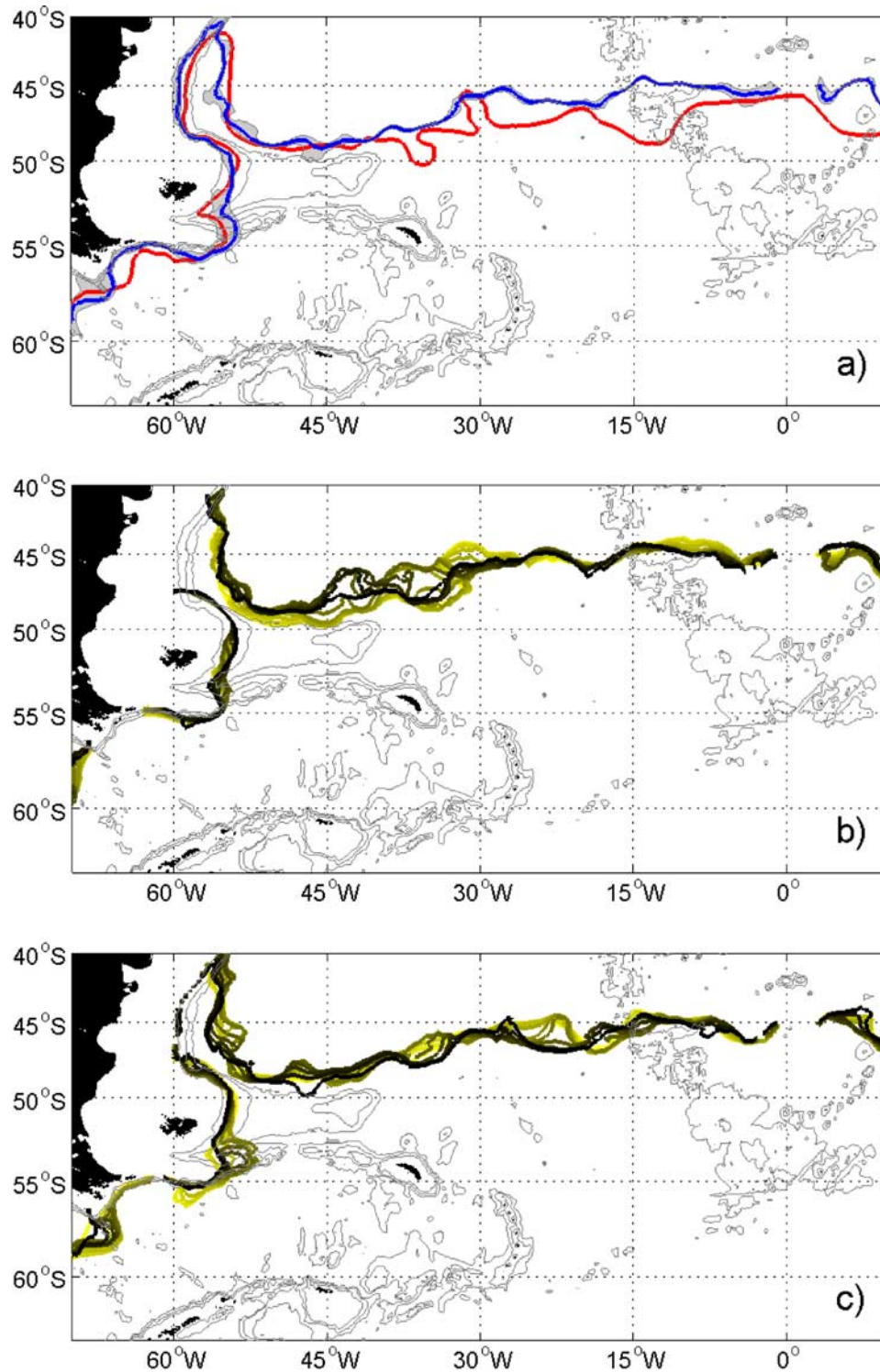


**Figure 8.** Position of the Subantarctic Front during 2004 and 2005. Isobaths are 1000, 2000, and 3000 m and land is shaded black. (a) Mean position of the Subantarctic Front (blue) and mapping error (grey) of the interpolation scheme. Position of the front by *Orsi et al.* [1995] in red. (b) Monthly position of the Subantarctic Front in 2004 (yellow to black). (c) Monthly position of the Subantarctic Front in 2005 (yellow to black).

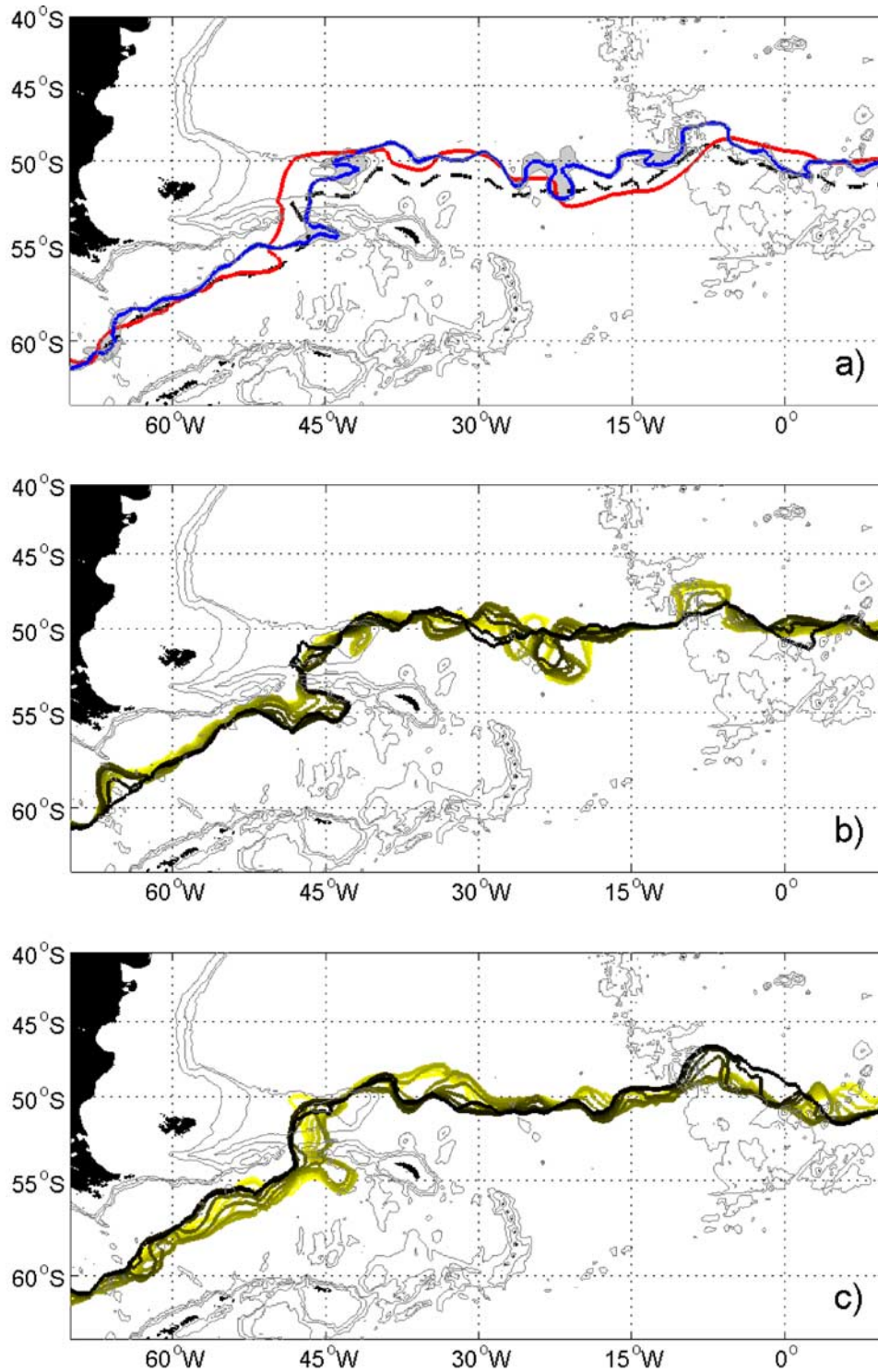


**Figure 9.** Position of the Polar Front during 2004 and 2005. Isobaths are 1000, 2000, and 3000 m and land is shaded black. (a) Mean position of the Polar Front (blue) and mapping error (grey) of the interpolation scheme. Position of the front by *Orsi et al.* [1995] in red and by *Moore et al.* [1999] in black. (b) Monthly position of the Polar Front in 2004 (yellow to black). (c) Monthly position of the Polar Front in 2005 (yellow to black).

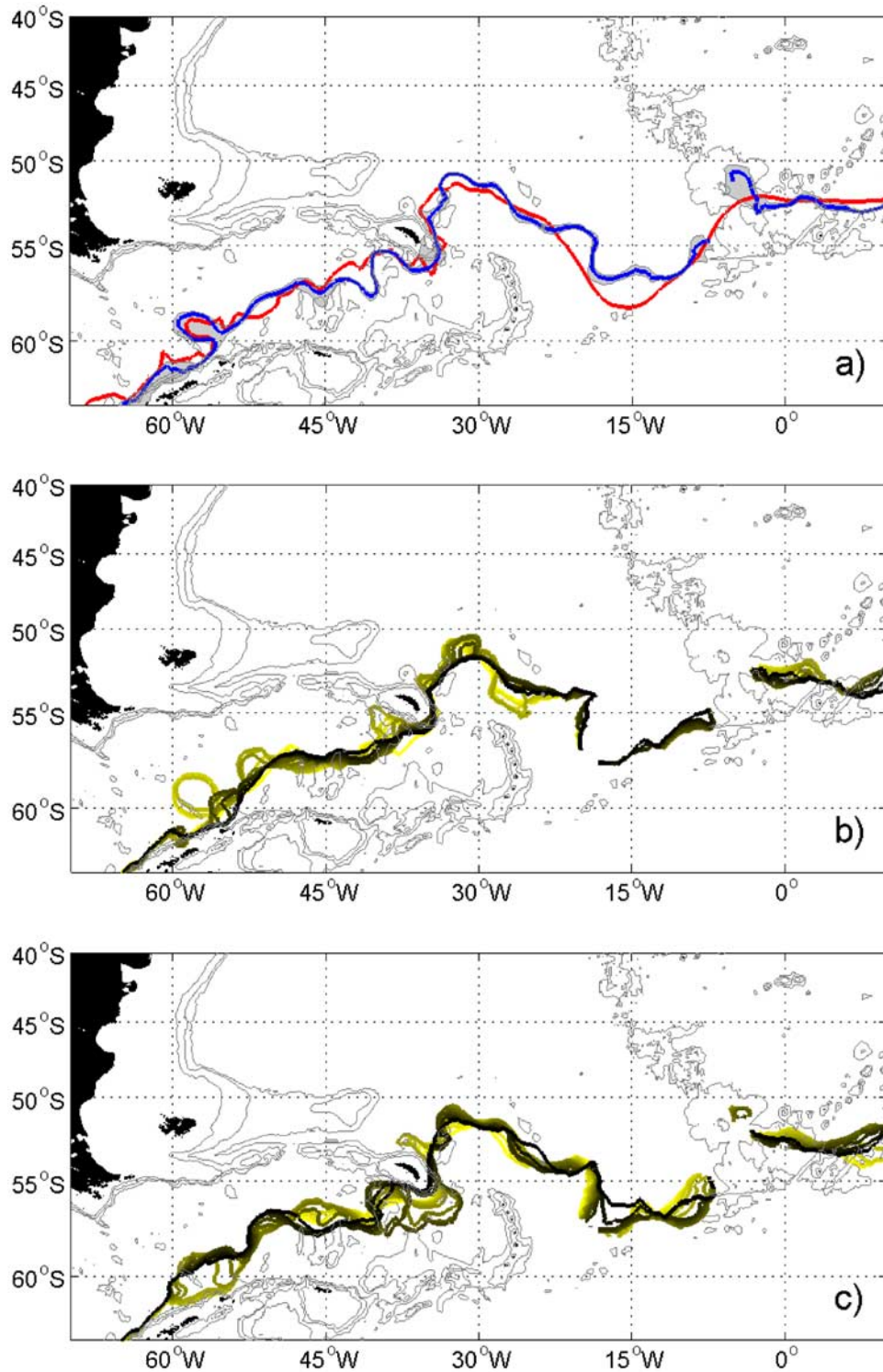


**Figure 10.** Position of the Southern ACC Front during 2004 and 2005. Isobaths are 1000, 2000, and 3000 m and land is shaded black. (a) Mean position of the SACCF (blue) and mapping error (grey) of the interpolation scheme. Position of the front by *Orsi et al.* [1995] modified by *Thorpe et al.* [2002] in red. (b) Monthly position of the SACCF in 2004 (yellow to black). (c) Monthly position of the SACCF in 2005 (yellow to black).

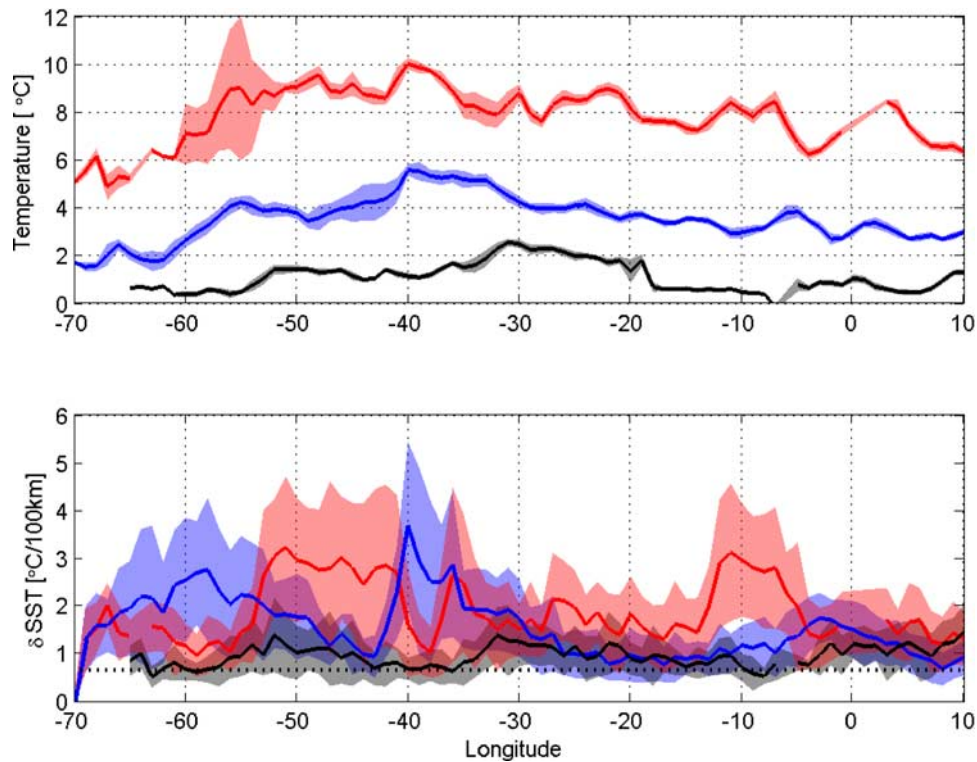


**Figure 11.** SST (top) and SST gradient (bottom) at frontal positions with mean as solid line and standard deviation as patch from monthly data for the period 2004–2005, inclusive. The SAF is in red, the PF in blue, and the SACCF in black. The dotted black line in the bottom panel shows the mean meridional increase in SST to the north.

western side of the Maurice Ewing Bank the PF showed strong variability in 2005. It then turned east following the topography. Immediately east of the Maurice Ewing Bank the PF started to meander up to  $3^\circ$  in latitude between  $42^\circ\text{W}$  and  $30^\circ\text{W}$ . This was further to the west than in 2004 (Figures 9b and 9c). It then crossed  $50^\circ\text{S}$ ,  $10^\circ\text{W}$  with strong variability on the east side of the Mid-Atlantic Ridge before following the bathymetry to the southeast (Figure 9c).

### 3.2.3. Southern ACC Front

[27] The average position of the SACCF is shown in Figure 10a. It is in good agreement with the frontal position of Orsi *et al.* [1995] modified by Thorpe *et al.* [2002]. The SACCF lies close to the shelf break of the Antarctic Peninsula (Figure 10a). It loops to the northwest north of Elephant Island, very similar to the positions of Orsi *et al.* The SACCF then meanders to the northeast toward the southwestern side of South Georgia. It wraps anticyclonically around South Georgia from the south and then retroflects north of the island across the Northeast Georgia Rise looping cyclonically to the southeast. At about  $57^\circ\text{S}$ ,  $15^\circ\text{W}$  it lies further north than in previous work [Orsi *et al.*, 1995]. The crossing of the Mid-Atlantic Ridge is not resolved because of lack of data (Figure 10a).

[28] The monthly positions reveal the high variability of the SACCF (Figures 10b and 10c). At the beginning of 2004, the SACCF showed a big cyclonic loop just east of the Shackleton Fracture Zone, which disappeared during 2004 (Figure 10b). It then meandered in a  $1^\circ$  wide band to the northeast. The area on the southwest side of South Georgia showed high variability in the frontal position, with

a cyclonic loop building up to the north and disappearing again during 2004. The front followed the continental shelf of South Georgia until the approximate region of the Northwest Georgia Rise, as per Meredith *et al.* [2003a]. Although an area of high variability, the SACCF seemed to be constrained by the Northeast Georgia Rise until it reaches its northernmost point at  $31^\circ\text{W}$ . It then turned southeastward until it reached  $54^\circ\text{S}$ ,  $20^\circ\text{W}$  where it turned sharply southward (Figure 10b). At  $58^\circ\text{S}$  it turned eastward again, but the lack of data in 2004 hampered resolution of the frontal position properly in this area. This lack of temporal resolution results in positions very close to the mean locations. We were able to map the SACCF again from  $52^\circ\text{S}$ ,  $5^\circ\text{W}$  from where it followed the north side of the SW Indian Ridge (Figure 10b).

[29] In 2005, the SACCF showed even more variability than in the previous year, with movements covering a range of  $3^\circ$  in latitude in the Scotia Sea (Figure 10c). Especially south of South Georgia the SACCF meandered and looped over a great range until it followed the shelf break on the east side of South Georgia. It then extended its position to the north of the island across the Northwest Georgia Rise during 2005 (Figure 10c). (This loop was already seen in Figure 6.) Again constrained by the Northeast Georgia Rise, the SACCF reached the northernmost point further to the west than in the previous year at about  $34^\circ\text{W}$ . It then turned southeastward but lay further north than in 2004. Again at  $54^\circ\text{S}$ ,  $20^\circ\text{W}$  it turned sharply southward showing high variability in crossing the ocean basin between the South Sandwich Islands and the Mid-Atlantic Ridge. The crossing

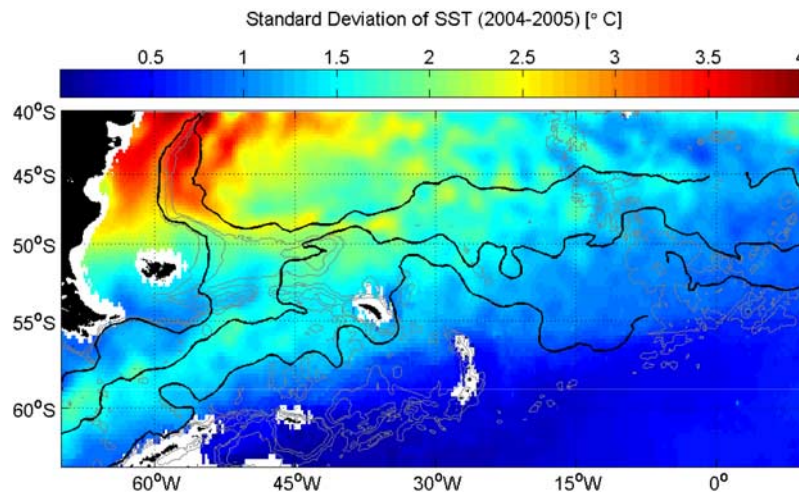


**Figure 12.** Standard deviation of daily SST data for the period 2004–2005, inclusive and the mean frontal positions of SAF, PF, and SACCF as derived by this study (solid lines). Isobaths are 1000, 2000, and 3000 m and land is shaded black.

of the Mid-Atlantic Ridge is not resolved in Figure 10c because of lack of data. The SACCF reappears again at 52°S, 5°W, possibly suggesting that the crossing is constrained by the bathymetry and follows the front of *Orsi et al.* [1995]. North of Bouvetøya the SACCF lay on the north side of the South West Indian Ridge (Figure 10c).

### 3.3. SST and SLA

[30] The satellite SST at the frontal positions is closely related to their meridional positions (Figure 11). The southernmost position of the SAF is in Drake Passage, where the SST is at its minimum of about 5°C. The same is true for the PF with an SST of below 2°C at the western edge of Drake Passage (Figure 11). Both fronts turn then sharply northward; this is reflected in the increasing SST at the front. The standard deviation of the SST increases because of the more meridional orientation of the front. During the northward loop of the SAF the SST expression rises from 6°C to 9°C between 60°–50°W. The SST of the PF increases between 50°–40°W from about 4°C to 6°C. The SSTs of the SAF and PF decrease by about 2°C to the east, although the fronts stay at the same latitude (PF) or even lie further north (SAF). The same is true for the SACCF but less pronounced and the SACCF lies further south in the east. The maximum SST of the SACCF is 2.5°C at 30°W with a drop to 0.5°C at 10°W (Figure 11). Figure 11 also shows the longitudinal distribution of the SST gradient. The SST gradient at the SACCF is around 1°C per 100 km, which is close to the 'normal' meridional increase in SST to the north. Over short time periods and small areas this gradient can be above this background noise, suggesting that the SACCF could occasionally be detected using remotely-sensed SST information as shown by *Meredith et al.* [2003b].

[31] When comparing the average frontal positions to the standard deviation of daily SST data for the period 2004 – 2005, it is obvious that the SAF and PF are in general associated with bands of high variability of SST (Figure 12). Although the seasonal cycle is included here, areas of high variability (>1.5°C) are related to meandering of the

fronts and eddy activity. On the contrary, areas with low standard deviation of SST indicate low variability of the frontal position and less eddy activity. The area southwest of Burdwood Bank along the continental shelf shows low variability in SST and coincides with low variability in the position of the SAF (Figure 8). This feature continues further north, where the SAF is again constrained by bathymetry along the shelf north of the Falklands (Figure 12). When the SAF turns southward, it is associated with stronger variability in SST, indicating higher variability of the frontal position, which we also found in our monthly positions (Figure 8). The band of high SST variability along the PF confirms the variability of the PF position from Drake Passage to the Mid-Atlantic Ridge (Figure 9). From Drake Passage to south of South Georgia the standard deviation of SST of 1.3°C coincides with the southernmost extent of the SACCF (Figure 10). On the eastern side of the island a patch of low SST variability indicates that the SACCF is constrained close to the shelf slope on this side of the island (Figure 12). However, north of the island the SST deviation increases related to a higher variability of the frontal position (Figure 10).

[32] The variance of sea level has been used for many years to identify regions of intense mesoscale variability [*Kostianoy et al.*, 2003]. Figure 13 shows the SLA variance calculated from weekly gridded altimeter data. In our area of interest are two regions of high SLA variance. The first one lies within the ACC in the Drake Passage south of the SAF and along the PF. This intense mesoscale variability shows that the PF in the Drake Passage is generally dominated by current meanders and mesoscale eddies. The other area of high SLA variance lies north of the mean SAF in the Brazil/Malvinas Confluence. This confluence of currents creates mesoscale meanders and eddies with energy levels ranked at the top of the world's oceans [*Fu et al.*, 2001; *Goni and Wainer*, 2001; *Vivier et al.*, 2001]. The mean SAF path is nestling to the west and south side of this area, indicating that all variability takes place north of the front. At around 40°W a transition zone starts where this

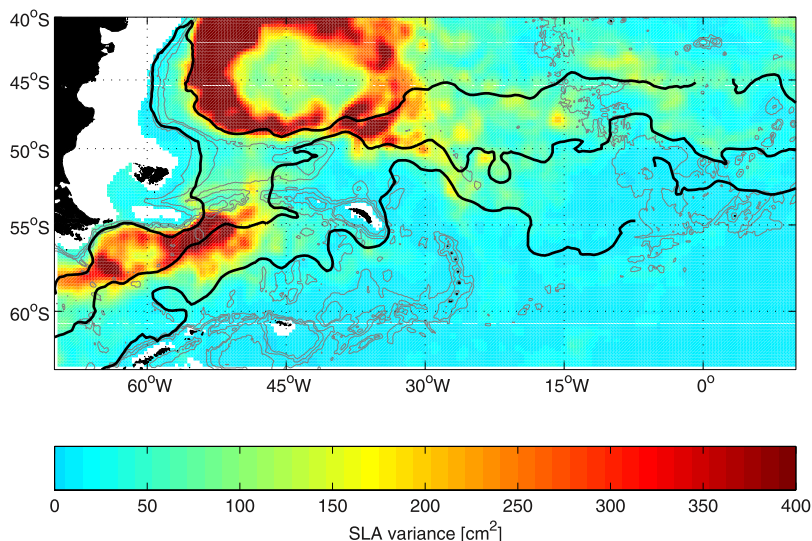


**Figure 13.** Variance of sea level anomaly based on weekly gridded altimeter data for the period August 2001–June 2006, inclusive. Mean frontal positions of SAF, PF, and SACCF as derived by this study. Isobaths are 1000, 2000, and 3000 m and land is shaded black.

energy is shifted from the north side of the SAF to the south, in particular in the vicinity of the SACCF at about 30–25°W.

## 4. Discussion

[33] In general, the average frontal positions derived from our data set are in agreement with previous work [Orsi *et al.*, 1995; Thorpe *et al.*, 2002], especially where the pathways are constrained by topography, e.g., at the North Scotia Ridge. However, some novel features are observed, which we outline here. First, we discuss the derived positions of the frontal system and its variability. Then, we examine the possible causes for the observed zonal shift of the ACC. Finally, we discuss the relationship between the surface and subsurface expressions of the three major fronts.

### 4.1. The Frontal Positions

[34] The main difference between our derived mean position of the SAF and the SAF location by Orsi *et al.* [1995] is the northward shift of up to 400 km east of 45°W. This could be the result of the slightly different temperature criteria used, but we compared our location with the 4°C isotherm at 200 dbar and 400 dbar, which are used for identification of the SAF in previous work [Peterson and Whitworth, 1989; Orsi *et al.*, 1993, 1995] to conclude that all criteria give very similar results. The SAF of Orsi *et al.* [1995] shows big loops to the south and north at about 37°W and 30°W. While our mean position does not show such features, the monthly positions reveal the high variability of the SAF in this region. The loops in Orsi *et al.* [1995] are based on a limited data set and show a snapshot of the SAF location, while we differentiate between a mean location and monthly snapshots. However, an interesting feature is that the monthly SAF positions east of the Maurice Ewing Bank are on average north of the SAF position by Orsi *et al.* [1995], indicating a northward shift of the northern boundary of the ACC in 2004 and 2005 when compared to the data available to Orsi *et al.* (Figure 8).

[35] Despite the differences in defining the PF, the mean PF paths from previous studies agree well with our observations, particularly in the vicinity of strong topographic features, such as the Drake Passage and the Mid-Atlantic Ridge. However, a relatively large difference is seen in the North Scotia Sea before the PF crosses the North Scotia Ridge. In 2004 and 2005, the PF extended far more to the east than in previous work, reaching nearly 42°W before looping back. The PF paths from Gille [1994] and Moore *et al.* [1999] lie also further to the east than the PF of Orsi *et al.* [1995], but not to such an extent. Our monthly PF positions also show high spatial variability in this area, but a longer time series is needed to verify if this eastward extent is particular to the studied time period or is a regular occurrence.

[36] The mean PF path is across the Maurice Ewing Bank, while two branches of higher SLA variance can be seen close to the west and south flanks of the Maurice Ewing Bank (Figure 13). This may result from a topographically-induced lateral splitting of the PF south of the bank as suggested by Naveira Garabato *et al.* [2002]. However, the monthly PF positions show that the PF loops cyclonically around the bank. The PF loops southward on the eastern side of the Maurice Ewing Bank in 2004, but not in 2005 (Figure 9). If this discrepancy is due to a lack of representativeness of the data used in Naveira Garabato *et al.* [2002] or in our data set needs further investigations on a smaller temporal and spatial scale.

[37] The monthly PF positions show also strong variability of the front due to meandering and meridional movements east of 45°W. Dong *et al.* [2006] suggested a correspondence between the tendency of the PF location and the meridional shift of the wind field, resulting in a move equatorward during winter. Our monthly positions do not support this, showing no seasonality in the monthly positions. This might be due to the fact that the short temporal variability is larger compared with the seasonal variability and that a seasonal signal is much smaller in the

subsurface expression than at the surface. Our PF positions show a high short-term variability due to meandering and eddy activity and we suggest that these eddies are much more important for the frontal position than the wind field.

[38] The SACCF shows great variability north of Elephant Island. Data from the WOCE section SR1b between 1993 and 2000 show that there are very often small, vertically-coherent eddies to the southern end of this section just north of Elephant Island [Cunningham *et al.*, 2003]. These eddies have the characteristics of water from south of the SB, but can be found almost as far north as the PF. This rich eddy field with associated low temperatures could be a factor in the high variability of the SACCF to the northwest of Elephant Island.

[39] Another interesting feature is the strong variability of the SACCF in the vicinity of South Georgia. The SACCF looped to the north before wrapping anticyclonically around South Georgia in early 2004. Meredith *et al.* [2005] used six years (1996–2001) of high-resolution hydrographic data collected during the austral summer to show the interannual variability of the water mass properties around South Georgia and concluded that significant variability occurs at subannual time scales. Indeed, our monthly SACCF positions show a high subannual variability (Figure 10). During the austral summer 2004/2005, the path of the SACCF moved further south, while the PF extended a loop along the North Scotia Ridge to the east before turning back to the west and crossing the North Scotia Ridge. At the end of 2005, the PF again lay further west, while the SACCF again looped northward before wrapping around South Georgia. This interplay and the strong variability north of the island, as shown in Figures 9 and 10, must have implications on the South Georgia ecosystem. We examine the potential impact of this physical variability on the local ecosystem separately using merged Argo/CTD-SRDL data (R. Saunders *et al.*, unpublished data, 2007).

[40] In 2004, the SAF shows strong meandering and eddy activity west of 30°W, while the PF shows the same further downstream east of 30°W. This transition takes place, where the two fronts are in close proximity, enhancing the baroclinic gradients and conditions favoring eddy formation. This is consistent with higher SLA variance in this region to as far south as the SACCF (Figure 13). Strong meandering and eddy activities are associated with the SAF from 45°–40°W, with the PF from 40°–30°W and with the SACCF around 30°–25°W. This “downstream” effect might be induced by eddies shed by the northerly front moving southwards, enhancing the baroclinic gradients even further, which in turn results in new eddy formation. This process would also transfer heat from the north to the south. This also supports the argument of Sun and Watts [2002], who suggested that the mean flow of the ACC transports heat from warm subtropical regions to cold subpolar regions. Sun and Watts [2002] also showed that the ACC warms in the western South Atlantic, cools until south of Africa, gaining heat again in the Indian Ocean and cools in the South Pacific. This heat loss is shown in Figure 11 by a decrease of SST of about 2°C to the east, although the fronts stay at the same latitude (PF) or even lie further north (SAF). The strong meandering in this area and frontal loops across the same longitude more than once cannot be resolved by using the methods of Dong *et al.* [2006] and

Moore *et al.* [1999]. This demonstrates the advantage of being able to track such movements of ACC fronts even more clearly using in-situ data.

#### 4.2. A Shift of the ACC

[41] Interestingly, the mean SAF, as positioned by our data set, crossed the Mid-Atlantic Ridge about 400 km further north than the SAF of Orsi *et al.* [1995]. The mean SACCF path follows the path by Orsi *et al.* [1995] and Thorpe *et al.* [2002] very closely, but at 15°W the SACCF lies further north. When the spatial resolution of our data set is best in this area (at the end of 2005), the SACCF was situated up to 150 km further north when compared to the location of Orsi *et al.* [1995]. The SAF and SACCF are deep reaching fronts and are constrained by the bathymetry in many places. This change from one constrained passing place to another one further north suggests a major shift in the location of the ACC between Orsi *et al.* [1995] and our findings.

[42] It has been argued that such shifts can happen in response to changes in wind stress. Such changes have been happening in recent decades. For example, Thompson and Solomon [2002] show an increased strength of the zonal winds over the Southern Ocean in the past three decades. A recent study argued that this will be followed by a significant increase in transport and a poleward change in position of the ACC [Fyfe and Saenko, 2006]. However, Meredith and Hogg [2006] cast doubt on whether this process described by Fyfe and Saenko [2006] is real or an artifact of coarse-resolution climate models. Contrary to Fyfe and Saenko [2006], we see a northward shift of the ACC in some locations in 2004 and 2005, when compared to previous work. Our findings suggest that the effect of eddies on the variability of the frontal positions is much more important than the seasonal wind field. This strengthens the argument of Meredith and Hogg [2006] that the zonal wind stress has no direct long term impact on the location and transport of the ACC. According to Meredith and Hogg [2006], eddies act to constrain such changes of the ACC that occur when changes in wind forcing occur. Nevertheless, Dong *et al.* [2006] suggest that there is observational evidence for this process. A northward shift of the maximum zonal wind stress may also force the PF to move to the north with variations in the wind field leading variations in the PF path [Dong *et al.*, 2006]. Changes in the wind field on time scales shorter than seasonal can change the ACC transport [Aoki, 2002; Hughes *et al.*, 2003] and therefore might alter the frontal positions.

#### 4.3. Correlations Between the Surface and Subsurface Expressions

[43] Some of the previous studies used satellite SST to define the positions of the ACC fronts. While this can be appropriate for the SAF, and to a lesser extent the PF, it could be quite difficult for determining the SACCF position (Figure 11). Nevertheless, Meredith *et al.* [2003b] showed an SST signal that was associated with the SACCF close to South Georgia, indicating the potential of SST for remote detection of this front for certain times and places.

[44] Consistent with previous studies, Dong *et al.* [2006] and others suggested that the surface PF location tends to be south of the subsurface PF location. Figure 9a supports this

argument, showing our derived locations of the PF generally north of the PF locations of *Moore et al.* [1999]. Admittedly, the topography seems to play an important role. Our comparisons between the PF positions and satellite SST data showed that when the PF path is constrained by topography, the SST gradient is high, suggesting a concurrence of surface and subsurface locations. However, over deep ocean basin regions with weak topographic variations, the PF meanders substantially, and the SST gradient is weak [*Moore et al.*, 1999; *Dong et al.*, 2006].

[45] The SST gradient at the PF in Figure 11 varies between  $1^{\circ}\text{C}$  and  $3.5^{\circ}\text{C}$  with a peak of more than  $5^{\circ}\text{C}$ , which is similar to *Dong et al.* [2006]. Interestingly *Moore et al.* [1999] show a peak in the SST gradient for the PF from the Drake Passage to  $20^{\circ}\text{W}$ , while we found two peaks, one at  $60^{\circ}\text{W}$  and another one at  $40^{\circ}\text{W}$ . The minimum is in between where the PF crosses the North Scotia Ridge. Either the SST gradient is very small or the surface and subsurface expression of the PF are different here. We suggest the latter, because this is also the place with the biggest differences between our mean path and the path based on the surface expression by *Moore et al.* [1999] (Figure 9a). Also to the east of  $30^{\circ}\text{W}$  the SST gradient of the PF is very weak, suggesting a higher separation between the surface and subsurface expression. Here the small SST gradient of the SAF suggests a separation between the surface and subsurface expression too. The SST gradient of the SAF is relatively weak except at two locations, where the SAF is constrained by the topography at  $50\text{--}40^{\circ}\text{W}$  north of the Falkland Plateau and at  $10^{\circ}\text{W}$  after crossing the Mid-Atlantic Ridge. This feature is also present in the PF and SACCF east of the Mid-Atlantic Ridge. However, all fronts show high SST gradients when they reach their northernmost point (Figure 11).

## 5. Summary

[46] Analysis of in-situ hydrographic data of the years 2004 and 2005 in the southwest Atlantic sector of the Southern Ocean has produced maps of the SAF, PF and SACCF within the ACC at high spatial and temporal resolution. The availability of Argo float data and the complementary CTD-SRD data have allowed us to examine the fronts simultaneously in much more detail than previously possible. In defining the fronts, we have placed most weight on the distribution of horizontal temperature gradients. Defining the fronts in this way corresponds to various scalar criteria used by earlier investigators. The data collected by animal-borne CTD-SRDs proved to be very useful in obtaining several cross-sections of the ACC at different locations and seasons. The existence of suitable proxies expressed in terms of subsurface temperature or satellite SST has allowed us to examine the spatial and temporal variability of the front locations. The results can be summarised as follows:

[47] 1. New technology has enabled us to produce an in-situ data set with high temporal and spatial resolution even in the Southern Ocean. The Global Ocean Observing System required the establishment of Argo, which is designed for broad-scale ocean sampling. Smaller scale eddy-resolving sampling is complementary to the broad-scale mode and can be achieved by using autonomous CTD-

Satellite Relay Data Loggers, which can be attached to marine animals. These high-accuracy sensors proved to have the ability to collect large numbers of profiles cost-effectively particularly in regions where traditional oceanographic measurements are scarce. They are a powerful complement to the array of Argo floats. Both technologies send data via satellites and have a great potential for observing the ocean in real-time, when used in tandem.

[48] 2. Our comprehensive data set enabled us to map the monthly positions of the SAF, PF and SACCF in 2004 and 2005. This time series indicates areas of high variability in these frontal locations. The SAF is constrained by the South American continental shelf, but shows high variability west of the Burdwood Bank and when crossing the ocean basin between South America and the Mid-Atlantic Ridge. The PF is the most active front with meandering along its entire path through our study region. It is constrained by the North Scotia Ridge and the Mid-Atlantic Ridge. The mean path of the PF is across the Maurice Ewing Bank, although SLA variance suggests two branches to the west and south of the bank. This needs further investigations on a smaller scale. The SACCF shows high variability in the Scotia Sea and to the northeast of South Georgia, but it is also constrained by specific topographic features. All frontal variability seems to be much more influenced by meandering and eddies than possible seasonality in the wind field. The spatial pattern of higher variability changes between the two years.

[49] 3. The position of the PF is highly variable south of the North Scotia Ridge. The front also extends much further to the east before crossing the North Scotia Ridge than in previous work. The extension of this eastward loop varies over time with the greatest extent in austral summer 2004/2005. The SACCF shows a northward loop on the west side of South Georgia before wrapping around the island. Again the size of this loop is highly variable with its peaks in winter 2004 and at the end of 2005. Whether these two frontal features are coupled needs further investigations.

[50] 4. After looping anticyclonically around South Georgia, the SACCF shows a strong variability in the position of its retroflexion north of the island. This tongue of the SACCF has its greatest extent to the west during winter. In 2004, this feature is less pronounced than in 2005, where it reached the Northwest Georgia Rise. Despite the meandering, the SACCF is constrained by the South Georgia shelf, the Northeast Georgia Rise and the Mid-Atlantic Ridge.

[51] 5. Previous studies were limited by the sparse hydrographic data in the Southern Ocean or were constrained by the continuity of the SST at the fronts when using satellite SST maps. The frontal positions based on the subsurface expressions within this study are compared to satellite SST. The SST gradient is in general the highest when the fronts are constrained by the bathymetry, induced by the concurrence of the surface and subsurface expression.

[52] 6. SST and SLA variance support the argument that there is a transition zone starting around  $40^{\circ}\text{W}$  where eddy energy is shifted from the north side of the SAF to the south, in particular in the vicinity of the SACCF at about  $30^{\circ}\text{--}25^{\circ}\text{W}$ .

[53] 7. East of  $40^{\circ}\text{W}$ , all three fronts were shifted further to the north than historical positions suggested, varying between 400 km for the SAF and 150 km for the SACCF.

This northward shifting of the ACC would not have been expected from previous work.

## Appendix

[54] All hydrographic data are used to generate horizontal temperature fields. To calculate the best estimate of temperature at each grid point, an optimal interpolation scheme similar to the one introduced by *Boehme and Send* [2005] is used. At each grid point the objective estimate of temperature  $T^{obj}$  is then given by:

$$T^{obj} = \langle \mathbf{d} \rangle + \omega \cdot (\mathbf{d} - \langle \mathbf{d} \rangle), \quad (\text{A1})$$

where  $\mathbf{d} = [d_1, \dots, d_n]$  denotes the set of temperature values,  $\langle \mathbf{d} \rangle$  denotes the mean value of the set of  $\mathbf{d}$  and  $\omega$  is the weighting matrix. We assume the covariance of the data  $\mathbf{d}$  to be exponential. However, the flow of the ACC follows the topography and a Gaussian function is not satisfactory. To take the complex topography into account each in-situ profile is weighted by three distances: the spatial distance  $\mathbf{D}$ , the fractional distance in potential planetary vorticity  $\mathbf{F}$  and the temporal distance  $\Delta t$  to the grid point *Davis* [1998];

$$\begin{aligned} D &= |\mathbf{0} - \mathbf{I}| \\ F &= \frac{|PV(\mathbf{0}) - PV(\mathbf{I})|}{\sqrt{PV^2(\mathbf{0}) + PV^2(\mathbf{I})}} \\ \Delta t &= |t_0 - t_I|. \end{aligned} \quad (\text{A2})$$

In equation (A2) the position  $(x_i, y_i)$  of the in-situ data point is given in  $\mathbf{I}$  and the date in  $t_I$ , while the grid point position is  $\mathbf{0}$  and the date  $t_0$ .  $\mathbf{D}$  is the spatial distance between the two points.  $\mathbf{F}$  takes account of the differences in barotropic potential vorticity  $\mathbf{PV}$ :

$$PV = \frac{f}{H}, \quad (\text{A3})$$

with the planetary vorticity  $f$  and the water depth  $H$  (taken from the 5-minute gridded global relief data TerrainBase (<http://www.ngdc.noaa.gov>). The PV criterion might be misleading in some cases, as two points with similar potential vorticity but lying in different basins separated by a ridge could have very different properties. This problem also exists when using a simple Gaussian mapping scheme. The modification by introducing the potential planetary vorticity into the mapping scheme gives superior results as outlined in *Boehme and Send* [2005].

[55] The covariance is a function of the temporal and spatial separation, and the exponential decay scale is determined by the spatial scale  $\lambda$  [km], the cross-isobathic scale  $\Phi$  [dimensionless], as well as the temporal scale  $\tau$  [days] [*Wong et al.*, 2003; *Boehme and Send*, 2005]. The covariance matrix for the temperature–grid data ( $Cdg$ ) and the temperature–temperature covariance matrix ( $Cdd$ ) then take the form:

$$\begin{aligned} Cdd_{ij}(x, y, t) &= \langle \mathbf{s}^2 \rangle \cdot \exp \left\{ - \left[ \frac{D_{ij}}{\lambda} + \frac{F_{ij}}{\Phi} + \frac{\Delta t^2}{\tau^2} \right] \right\}, \\ Cdg_i(x, y, t) &= \langle \mathbf{s}^2 \rangle \cdot \exp \left\{ - \left[ \frac{D_{i0}}{\lambda} + \frac{F_{i0}}{\Phi} + \frac{\Delta t^2}{\tau^2} \right] \right\}. \end{aligned} \quad (\text{A4})$$

$\langle \mathbf{s}^2 \rangle$  is the signal variance of the temperature data. The inverse solution then is *McIntosh* [1990]

$$\omega = Cdg \cdot [Cdd + I \cdot \langle \eta^2 \rangle]^{-1}, \quad (\text{A5})$$

where  $\mathbf{I}$  denotes the identity matrix.

[56] The scale parameters used for objective mapping are as important as the method itself, as they will represent the hydrographic structure of the ocean, hence it is necessary to calculate these scale parameters from the correlation function of in-situ measurements.

[57] According to the objective mapping method used a time-independent spatial scale, a cross-isobath scale and a temporal scale are required. Following *Boehme and Send* [2005], the normalized autocorrelation function  $R(D, F)$  is calculated and then fitted by an exponential distribution, which yields the scaling parameters  $\lambda$  and  $\Phi$  set to  $\lambda = 200$  km and  $\Phi = 0.3$ . Due to a lack of reliable information with which to calculate the temporal scale, we instead used daily SST data. Using these data, processes with time scales from one day to two years are resolved. Again we followed the method of *Boehme and Send*, which yields a temporal scale of  $\tau = 112$  days.

[58] This interpolation scheme is used to calculate the potential temperature field on different depth levels. All these calculations are done on a  $0.4^\circ \times 0.25^\circ$  grid ( $\sim 25$  km) from  $80^\circ\text{W}$  to  $15^\circ\text{E}$  and  $63^\circ\text{S}$  to  $40^\circ\text{S}$ . The first run used all available Argo and CTD-SRDL data from 2004 and 2005 with no time scale to calculate the average temperature field of this time period. We mapped temperature fields at 200, 300 and 500 dbar depths and the temperature of the temperature minimum layer. To avoid eddy-like features we only used the most unbroken isotherms from west to east.

[59] To resolve the high temporal variability of the fronts, we used the same scheme to calculate the frontal positions on a monthly basis. Using the detected temporal scale  $\tau$ , we mapped the temperature fields to the middle of each month in 2004 and 2005 and extracted the dedicated isotherms. This gives us 24 monthly positions for each front from January 2004 to December 2005.

[60] **Acknowledgments.** We thank C. Duck, I. Field, K. Bennett and S. Moss for their help on deploying CTD-SRDLs on South Georgia. We thank the two anonymous reviewers for their helpful comments. Float data were collected and made freely available by the International Argo Project and the national program that contribute to it (<http://www.argo.net>). Argo is a pilot program of the Global Ocean Observing System. Microwave OI SST data are produced by Remote Sensing Systems and sponsored by the National Oceanographic Partnership Program (NOPP), the NASA Earth Science Physical Oceanography Program, and the NASA REASON DISCOVER Project. Data are available at [www.remss.com](http://www.remss.com). The altimeter products were produced by SSALTO/DUACS and distributed by AVISO with support from CNES. This research was funded by NERC grant NER/D/S/2002/00426 and a NERC CASE Ph.D. studentship between the University of St. Andrews and the British Antarctic Survey.

## References

- Aoki, S. (2002), Coherent sea level response to the antarctic oscillation, *Geophys. Res. Lett.*, 29(20), 1950, doi:10.1029/2002GL015733.  
 Bailleul, F., J.-B. Charrassin, P. Monestiez, F. Roquet, M. Biuw, and C. Guinet (2007), Successful foraging zones of southern elephant seals from the Kerguelen Islands in relation to oceanographic conditions, *Phil. Trans. R. Soc. B.*, 362, 1487, doi:10.1098/rstb.2007.2109.  
 Belkin, I. M., and A. L. Gordon (1996), Southern Ocean fronts from the Greenwich meridian to Tasmania, *J. Geophys. Res.*, 101(C2), 3675–3696.

- Biuw, M., et al. (2007), Variations in behavior and condition of a Southern Ocean top predator in relation to in situ oceanographic conditions, *Proc. Natl. Acad. Sci. U.S.A.*, *104*, 13,705–13,710, doi:10.1073/pnas.0701121104.
- Boehme, L., and U. Send (2005), Objective analyses of hydrographic data for referencing profiling float salinities in highly variable environments, *Deep Sea Res., Part II*, *52*, 651–664, doi:10.1016/j.dsr2.2004.12.014.
- Boehme, L., S. E. Thorpe, M. Biuw, M. Fedak, and M.P. Meredith (2008), Monitoring Drake Passage with elephant seals: Frontal structures and snapshots of transport, *Limnology and Oceanography*, *53*(5), 2350–2360.
- Botnikov, V. N. (1963), Geographical position of the antarctic convergence zone in the Southern Ocean (in Russian), *Sov. Antarct. Exped. Inf. Bull.*, *4*(41), 324–327, English Trans.
- Boyd, J. D., and R. Linzell (1993), The temperature and depth accuracy of Sippican T-5 XBTs, *J. Atmos. Ocean. Technol.*, *10*, 128–136, doi:10.1175/1520-0426.
- Charrassin, J.-B., Y.-H. Park, Y. Le Maho, and C.-A. Bost (2004), Fine resolution 3d temperature fields off Kerguelen from instrumented penguins, *Deep Sea Res., Part I*, *51*, 2091–2103, doi:10.1016/j.dsr.2004.07.019.
- Cunningham, S. A., S. G. Alderson, B. A. King, and M. A. Brandon (2003), Transport and variability of the Antarctic Circumpolar Current in Drake Passage, *J. Geophys. Res.*, *108*(C5), 8084, doi:10.1029/2001JC001147.
- Davis, R. E. (1998), Preliminary results from directly measured middepth circulation in the tropical and South Pacific, *J. Geophys. Res.*, *103*(C11), 24,619–24,639.
- Dong, S., J. Sprintall, and S. T. Gille (2006), Location of the Antarctic Polar Front from AMSR-E Satellite sea surface temperature measurements, *J. Phys. Oceanogr.*, *36*(11), 2075–2089, doi:10.1175/JPO2973.1.
- Ducet, N., P. Y. L. Traon, and G. Reverdin (2000), Global high-resolution mapping of ocean circulation from TOPEX/Poseidon and ERS-1 and -2, *J. Geophys. Res.*, *105*, 19,477–19,498.
- Evans, W. E. (1970), Uses of advanced space technology and upgrading the future of oceanography, in *AIAA Paper*, 7-01273, 3 pp.
- Fu, L.-L., B. Cheng, and B. Qiu (2001), 25-day period large-scale oscillations in the argentine basin revealed by the TOPEX/Poseidon altimeter, *J. Phys. Oceanogr.*, *31*(2), 506–517, doi:10.1175/1520-0485.
- Fyfe, J. C., and O. A. Saenko (2006), Simulated changes in the extratropical Southern Hemisphere winds and currents, *Geophys. Res. Lett.*, *33*, L06701, doi:10.1029/2005GL025332.
- Gentemann, C. L., F. J. Wentz, C. A. Mears, and D. K. Smith (2004), In situ validation of tropical rainfall measuring mission microwave sea surface temperatures, *J. Geophys. Res.*, *109*, C04021, doi:10.1029/2003JC002092.
- Gille, S. T. (1994), Mean sea surface height of the Antarctic Circumpolar Current from GEOSAT data: Methods and application, *J. Geophys. Res.*, *99*(18), 18,255–18,273.
- Goni, G. J., and I. Wainer (2001), Investigation of the Brazil Current Front variability from altimeter data, *J. Geophys. Res.*, *106*(C12), 31,117–31,128.
- Gordon, A. L. (1971), Antarctic Polar Frontal zone, in *Antarctic Oceanology I, Antarct. Res. Ser.*, vol. 15, edited by J. L. Reid, pp. 205–221, AGU, Washington, D. C.
- Gould, J., et al. (2004), Argo profiling floats bring new era of in situ ocean observations, *Eos Trans. AGU*, *85*(19), doi:10.1029/2004EO190002.
- Hughes, C. W., P. L. Woodworth, M. P. Meredith, V. Stepanov, T. Whitworth, and A. R. Pyne (2003), Coherence of Antarctic sea levels, Southern Hemisphere annular mode, and flow through Drake Passage, *Geophys. Res. Lett.*, *30*(9), 1464, doi:10.1029/2003GL017240.
- Kostianoy, A. G., A. I. Ginzburg, S. A. Lebedev, M. Frankignoulle, and B. Delille (2003), Fronts and mesoscale variability in the southern Indian Ocean as inferred from the TOPEX/POSEIDON and ERS-2 altimetry data, *Oceanology*, *43*(5), 632–642.
- Le Traon, P.-Y., and G. Dibarboure (1999), Mesoscale mapping capabilities of multi-satellite altimeter missions, *J. Atmos. Ocean. Technol.*, *16*, 1208–1223.
- Le Traon, P.-Y., G. Dibarboure, and N. Ducet (2001), Use of a high-resolution model to analyze the mapping capabilities of multiple-altimeter missions, *J. Atmos. Ocean. Technol.*, *18*, 1208–1223.
- Lydersen, C., O. A. Nøst, K. M. Kovacs, and M. A. Fedak (2004), Temperature data from Norwegian and Russian waters of the northern Barents Sea collected by free-living ringed seals, *J. Mar. Syst.*, *46*, 99–108.
- Lydersen, C., O. A. Nøst, P. Lovell, B. J. McConnell, T. Gammelsrød, C. Hunter, M. A. Fedak, and K. M. Kovacs (2002), Salinity and temperature structure of a freezing Arctic fjord monitored by white whales (*Delphinapterus leucas*), *Geophys. Res. Lett.*, *29*(23), 2119, doi:10.1029/2002GL015462.
- McIntosh, P. C. (1990), Oceanographic data interpolation: Objective analysis and splines, *J. Geophys. Res.*, *95*(C8), 13,529–13,541.
- Meredith, M. P., and A. M. Hogg (2006), Circumpolar response of Southern Ocean eddy activity to a change in the southern annular mode, *Geophys. Res. Lett.*, *33*, L16608, doi:10.1029/2006GL026499.
- Meredith, M. P., J. L. Watkins, E. J. Murphy, N. J. Cunningham, A. G. Wood, R. Korb, M. J. Whitehouse, S. E. Thorpe, and F. Vivier (2003a), An anticyclonic circulation above the Northwest Georgia Rise, Southern Ocean, *Geophys. Res. Lett.*, *30*(20), 2061, doi:10.1029/2003GL018039.
- Meredith, M. P., J. L. Watkins, E. J. Murphy, P. Ward, D. G. Bone, S. E. Thorpe, S. A. Grant, and R. S. Ladkin (2003b), Southern ACC Front to the northeast of South Georgia: Pathways, characteristics, and fluxes, *J. Geophys. Res.*, *108*(C5), 3162, doi:10.1029/2001JC001227.
- Meredith, M. P., M. A. Brandon, E. J. Murphy, P. N. Trathan, S. E. Thorpe, D. G. Bone, P. P. Chernyshkov, and V. A. Sushin (2005), Variability in hydrographic conditions to the east and northwest of South Georgia, 1996–2001, *J. Mar. Syst.*, *53*, 143–167, doi:10.1016/j.jmarsys.2004.05.005.
- Moore, J. K., M. R. Abbott, and J. G. Richman (1999), Location and dynamics of the Antarctic Polar Front from satellite sea surface temperature data, *J. Geophys. Res.*, *104*(13), 3059–3074.
- Naveira Garabato, A. C., K. J. Heywood, and D. P. Stevens (2002), Modification and pathways of Southern Ocean deep waters in the Scotia Sea, *Deep Sea Res., Part I*, *49*(4), 681–705, doi:10.1016/S0967-0637(01)00071-1.
- Nowlin, W. D., and M. Clifford (1982), The kinematic and thermohaline zonation of the Antarctic Circumpolar Current at Drake Passage, *J. Mar. Res.*, *40*, 481–507.
- Nowlin, W. D., and J. M. Klinck (1986), The physics of the Antarctic Circumpolar Current, *Rev. Geophys.*, *24*(3), 469–491.
- Nowlin, W. D., T. Whitworth III, and R. D. Pillsbury (1977), Structure and transport of the Antarctic Circumpolar Current at Drake Passage from short-term measurements, *J. Phys. Oceanogr.*, *7*, 778–802.
- Orsi, A. H., T. Whitworth III, and W. D. Nowlin (1995), On the meridional extent and fronts of the Antarctic Circumpolar Current, *Deep Sea Res., Part I*, *42*(5), 641–673.
- Orsi, A. H., W. D. Nowlin, and T. Whitworth III (1993), On the circulation and stratification of the Weddell Gyre, *Deep Sea Res., Part I*, *40*(1), 169–203.
- Peterson, R. G., and T. Whitworth III (1989), The Subantarctic and Polar Fronts in relation to deep water masses through the southwestern Atlantic, *J. Geophys. Res.*, *94*(C8), 10,817–10,838.
- Rintoul, S. R., C. W. Hughes, and D. Olbers (2001), The Antarctic Circumpolar Current system, in *Ocean Circulation and Climate: Observing and Modelling the Global Ocean*, edited by G. Siedler, J. Church, and J. Gould, pp. 271–302, Elsevier, New York.
- Sievers, H. A., and W. D. Nowlin Jr. (1984), The stratification and water masses at Drake Passage, *J. Geophys. Res.*, *89*(C6), 10,489–10,514.
- Sokolov, S., and S. R. Rintoul (2002), Structure of Southern Ocean fronts at 140°E, *J. Mar. Syst.*, *37*, 151–184, doi:10.1016/S0924-7963(02)00200-2.
- Sokolov, S., and S. R. Rintoul (2007), Multiple jets of the Antarctic Circumpolar Current south of Australia, *J. Phys. Oceanogr.*, *37*(5), 1394–1412, doi:10.1175/JPO3111.1.
- Sokolov, S., S. R. Rintoul, and B. Wienecke (2006), Tracking the Polar Front south of New Zealand using penguin dive data, *Deep Sea Res., Part I*, *53*(4), 591–607, doi:10.1016/j.dsr.2005.12.012.
- Sun, C., and D. R. Watts (2002), Heat flux carried by the Antarctic Circumpolar Current mean flow, *J. Geophys. Res.*, *107*(C9), 3119, doi:10.1029/2001JC001187.
- Thompson, D. W. J., and S. Solomon (2002), Interpretation of recent Southern Hemisphere climate change, *Science*, *296*, 895–899, doi:10.1126/science.1069270.
- Thorpe, S. E., K. J. Heywood, M. A. Brandon, and D. P. Stevens (2002), Variability of the Southern Antarctic Circumpolar Current Front north of South Georgia, *J. Mar. Syst.*, *37*, 85–105.
- Vivier, F., C. Provost, and M. P. Meredith (2001), Remote and local forcing in the Brazil/Malvinas region, *J. Phys. Oceanogr.*, *31*, 892–913.
- Whitworth, T. (1980), Zonation and geostrophic flow of the Antarctic Circumpolar Current at Drake Passage, *Deep Sea Res.*, *21*, 497–507.
- Wong, A. P. S., G. C. Johnson, and W. B. Owens (2003), Delayed-mode calibration of autonomous CTD profiling float salinity data by  $\Theta$ -S climatology, *J. Atmos. Ocean. Technol.*, *2*, 308–318.

M. Biuw, L. Boehme, and M. Fedak, NERC Sea Mammal Research Unit, Gatty Marine Laboratory, University of St. Andrews, St. Andrews, Fife KY16 8LB, UK. (lb284@st-andrews.ac.uk)

M. P. Meredith and S. E. Thorpe, British Antarctic Survey, Natural Environment Research Council, High Cross, Madingley Road, Cambridge CB3 0ET, UK.